Fluorescent vibration-rotation excitation of cometary C2

Gredel, R.; Dishoeck, E.F. van; Black, J.H.

THE ASTROPHYSICAL JOURNAL, 338:1047–1070, 1989 March 15

FLUORESCENT VIBRATION-ROTATION EXCITATION OF COMETARY C_2[1]

ROLAND GREDEL AND EWINE F. VAN DISHOECK[2]
Harvard-Smithsonian Center for Astrophysics

AND

JOHN H. BLACK
Steward Observatory, University of Arizona
Received 1987 December 23; accepted 1988 August 25

ABSTRACT

The statistical equilibrium equations that determine the population densities of the energy levels in cometary C_2 molecules due to fluorescent excitation are examined in detail. The main differences with previous models are that the present calculations take the rotation structure of the transitions explicitly into account and that they use a detailed solar spectrum. Synthetic spectra are computed as functions of the strengths of two poorly determined molecular properties, the $a\,^3\Pi_u$–$X\,^1\Sigma_g^+$ and the $c\,^3\Sigma_u^+$–$X\,^1\Sigma_g^+$ intercombination transition moments $|D_{a-X}|^2$ and $|D_{c-X}|^2$. It is found that the magnitude of the $a\,^3\Pi_u$–$X\,^1\Sigma_g^+$ transition moment affects the vibrational temperatures in the singlet and triplet states, whereas both intercombination transitions influence the rotational temperatures in these states. The singlet to triplet population ratios are sensitive to the $c\,^3\Sigma_u^+$–$X\,^1\Sigma_g^+$ interaction as well. The calculated profiles are compared with high-resolution spectra of the ($v' = 0$, $v'' = 0$) Swan band in Comet Halley obtained in 1985 December at the MMT. The observations indicate a lower C_2 rotational excitation at the nucleus of the comet than at a sunward offset position in the coma. The observational data at the offset position can be well reproduced with $|D_{a-X}|^2 \approx 3.5 \times 10^{-6}$ a.u. and $|D_{c-X}|^2 \approx 3.5 \times 10^{-6}$–$2 \times 10^{-5}$ a.u., depending on the probabilities for the $d\,^3\Pi_g$–$c\,^3\Sigma_u^+$ emission. The parameters inferred from the Swan (0, 0) band measurements also reproduce other high-resolution observations of C_2 in Comet Halley, and can be used to simulate the entire visible C_2 spectrum. The recent detailed theoretical $a\,^3\Pi_u$–$X\,^1\Sigma_g^+$ transition probabilities of Le Bourlot and Roueff for low rotational levels are employed as well, and they are found to be slightly too small to cool the rotational and vibrational population distributions to the observed temperatures. Simple theoretical estimates for both intercombination transition moments are made based on recent ab initio calculations of the coupling matrix elements by Klotz and result in values that are also somewhat smaller than those inferred from the observations. Although the fluorescent process is the most likely excitation mechanism of cometary C_2, definite conclusions must await more accurate determinations of the intercombination transition probabilities.

Subject headings: comets — molecular processes — transition probabilities

I. INTRODUCTION

The emission lines of the C_2 $d\,^3\Pi_g$–$a\,^3\Pi_u$ Swan bands are among the most prominent features in cometary spectra, and the $\Delta v = v' - v'' = 0$, $+1$, and -1 band sequences dominate the visible part of the spectrum around 5000 Å. The observed line intensities depend on the populations of the vibration-rotation levels, which, in turn, are sensitive to the location of the comet with respect to the Sun, and to the physical conditions in the comet. Thus a detailed study of the population distribution may provide insight into the nature of the comet, and the mechanism that is responsible for the population of the energy levels.

It is commonly accepted that resonance fluorescence in the solar radiation field is the dominant excitation process of most cometary molecules, including C_2 (Stawikowski and Swings 1960; Arpigny 1965, 1976). Compared with other cometary molecules, C_2 has more highly populated excited vibration-rotation levels. This is due to the fact that $^{12}C_2$, a homonuclear molecule, has no permanent electric dipole moment, so that electric dipole transitions among vibrational levels within an electronic state are forbidden. If interactions with other electronic states were negligible, the vibrational temperature characterizing the level populations would thus be expected to approach the color temperature of the Sun, $T \approx 5800$ K (Stockhausen and Osterbrock 1965). This prediction is in conflict with observations of C_2 in a number of comets. In particular, low-resolution, $\lambda/\Delta\lambda \approx 500$, photoelectric measurements of the $\Delta v = 0$, 1, and -1 band sequences suggest that the populations of the higher vibrational levels in the $d\,^3\Pi_g$ state are characterized by a lower temperature than the lower levels (Mayer and O'Dell 1968; Gebel 1970; A'Hearn 1975). A low vibrational excitation temperature, $T_{vib} \approx 3500$ K, referring to all levels $v' = 1$–5 of the $d\,^3\Pi_g$ state, has also been found by Lambert and Danks (1983) from high-resolution, $\lambda/\Delta\lambda \approx 1.5 \times 10^4$, photoelectric spectra of comet West 1976 VI.

The discrepancy between observations and the simple resonance-fluorescence theory has stimulated a number of more extensive theoretical investigations. First, Krishna Swamy and O'Dell (1977) realized that the Swan $d\,^3\Pi_g$–$a\,^3\Pi_u$ bands cannot be treated as an isolated system, but that the upper $b\,^3\Sigma_g^-$ state of the Ballik-Ramsay system has to be included in the fluorescence cascade. As Figure 1 illustrates, vibrational levels with $v \geq 4$ in the $a\,^3\Pi_u$ state lie energetically higher than vibrational levels of the $b\,^3\Sigma_g^-$ state. Thus popu-

[1] Based on observations made with the Multiple Mirror Telescope, a joint facility of the University of Arizona and the Smithsonian Institution.
[2] Junior Fellow, Harvard Society of Fellows.

lation density in the $a\,^3\Pi_u$, $v_1 \geq 4$ levels can decay efficiently to lower vibrational levels in the $a\,^3\Pi_u$ state through two transitions in the Ballik-Ramsay system, namely $a\,^3\Pi_u(v_1 \geq 4) \rightarrow b\,^3\Sigma_g^-(v_2) \rightarrow a\,^3\Pi_u(v_3)$ with energies $E(v_1) > E(v_2) > E(v_3)$. With the inclusion of the $b\,^3\Sigma_g^-$ state, Krishna Swamy and O'Dell (1977) and A'Hearn (1978) found a decrease in the relative population densities $n(v)/n(v = 0)$ of the $d\,^3\Pi_g$ state with increasing v, in qualitative agreement with observations. Quantitatively, however, this cooling mechanism appeared insufficient to reproduce the measurements (Krishna Swamy and O'Dell 1977; Lambert and Danks 1983).

Spin-forbidden transitions to the ground $X\,^1\Sigma_g^+$ state can also act as an important cooling mechanism for the $a\,^3\Pi_u$ vibrational levels. Since intercombination transitions do not depend on the intensity of the solar radiation field, the vibrational ladder should be cooled more efficiently with increasing heliocentric distance, where the upward transitions in the Swan and Ballik-Ramsay systems that lead to the population of the high vibrational levels in $d\,^3\Pi_g$ becomes less rapid. Krishna Swamy and O'Dell (1979) included the $a\,^3\Pi_u$–$X\,^1\Sigma_g^+$ transition in their calculations by treating the ill-determined intercombination transition moment $|D_{a-X}|^2$ as a free parameter, but found no significant changes in the Swan $\Delta v = 1/\Delta v = 0$ flux ratios for small transition moments $|D_{a-X}|^2 \lesssim 10^{-5}$ atomic units (a.u.). The populations in the singlet states are, however, slightly sensitive to the strength of the singlet-triplet exchange rate. Unfortunately, observations of transitions involving singlet states of C_2, such as the Phillips $A\,^1\Pi_u$–$X\,^1\Sigma_g^+$ and Mulliken $D\,^1\Sigma_u^+$–$X\,^1\Sigma_g^+$ systems, are still limited, because these bands are relatively weak and occur in unfavorable parts of the spectrum (O'Dell 1971; A'Hearn and Feldman 1980; Danks and Dennefeld 1981; McFadden *et al.* 1987; Appenzeller and Münch 1987). The limited available measurements have been used to infer a value for the intercombination transition moment of $|D_{a-X}|^2 \approx 10^{-5}$ a.u. (Krishna Swamy and O'Dell 1979, 1981; A'Hearn and Feldman 1980), but the derived value depends strongly on the adopted oscillator strengths for the singlet transitions (Lambert and Danks 1983).

An estimate of the a–X transition moment has been made by Lambert and Danks (1983) on the basis of second-order perturbation theory. The predicted $|D_{a-X}|^2 \approx 10^{-7}$ a.u. for the (0, 0) band was significantly smaller than the value needed to cool the $d\,^3\Pi_g$ vibrational ladder to 3500 K, leading the authors to suggest that other depopulation transitions might play an important role. Among the proposed systems, the $c\,^3\Sigma_u^+$–$X\,^1\Sigma_g^+$ transition is the best candidate. The $c\,^3\Sigma_u^+$ state had previously been identified through its perturbations of the $a\,^3\Pi_u$ state, and electronic transitions involving this state have been seen in the laboratory only recently (van de Burgt and Heaven 1987). The $c\,^3\Sigma_u^+$–$X\,^1\Sigma_g^+$ transitions may lead to an effective transfer of population density from triplet to singlet states, since the metastable $c\,^3\Sigma_u^+$ state can be populated efficiently by the allowed $d\,^3\Pi_g$–$c\,^3\Sigma_u^+$ transition. However, taking the $c\,^3\Sigma_u^+$ state into account in their model, Krishna Swamy and O'Dell (1987) found no significant change in the vibrational temperature characterizing the triplet level populations, although a dependence of the singlet-triplet flux ratio on the d–c transition moment was noticed.

Most theoretical and observational discussions have centered on the vibrational excitation of the molecule. The rotational population distribution is much more difficult to determine observationally, since it requires high-resolution photoelectric spectra in which the rotational structure is resolved. Such data have been published only by Lambert and Danks (1983) for comet West 1976 VI for the $\Delta v = 1$ sequence from 4660 to 4750 Å. In this case, the rotational temperature $T_{\rm rot} \approx (3500 \pm 500)$ K was found to be low, and to be similar to the vibrational temperature. Previous suggestions of low rotational temperatures $T_{\rm rot} \approx 3000$–4000 K in comets were made by A'Hearn (1975) and Danylewich *et al.* (1978) on the basis of low-resolution spectra.

In the models developed so far (Krishna Swamy and O'Dell 1977, 1979, 1981, 1987; Krishna Swamy 1986; A'Hearn 1978), the statistical equilibrium equations were solved for the vibrational states only, and a smoothed solar radiation field was adopted for the evaluation of the absorption coefficients. The relative population densities of the individual levels were subsequently obtained by distributing the calculated population density of each vibrational state among its rotational levels under the assumption of a Boltzmann distribution. The population densities in the three triplet substates were assumed to be equal, and the rotational excitation temperature was usually assumed to be the same as the vibrational temperature. These models are useful for the investigation of the population distribution among the various vibrational states, but it is doubtful if they are appropriate to model the rotational structure, for a number of reasons. First, the intercombination transitions are the only radiative link between the singlet and triplet states, and they may introduce different population densities in the F_1, F_2, and F_3 triplet substates, as Lambert and Danks (1983) pointed out. More serious, however, is the assumption of similar vibrational and rotational excitation temperatures, since there is no *a priori* reason to assume that they are the same, except if the molecules were thermally excited. Finally, it is not proven beforehand that the rotational excitation can be understood in terms of resonance fluorescence as well, as seems to be the case for the vibrational excitation.

Since high-resolution photoelectric spectrometers have become available at various observatories in recent years, a large number of high-quality spectra is expected to result from the recent appearances of comet Giacobinni-Zinner in 1985, comet Halley in 1986, and comet Wilson in 1987 (Tegler and O'Dell 1987; Wehinger *et al.* 1986, 1989; Appenzeller and Münch 1987, Arpigny *et al.* 1986). The need to solve the statistical equilibrium equations for the rotational levels explicitly is thus evident. In addition, detailed theoretical calculations of the a–X intercombination transition moments for the individual F_1–F_3 rotational levels have recently appeared (Le Bourlot and Roueff 1986), as well as further experimental and theoretical determinations of other allowed and forbidden transition strengths (Bauer *et al.* 1985, 1986; Stark and Davis 1985; Klotz 1987; ONeil, Rosmus, and Werner 1987). These new data constrain the molecular parameters in the models significantly, and may allow a test of the basic assumption of resonance fluorescence as the main C_2 excitation mechanism.

Apart from the intrinsic fascination of a complicated fluorescence process, a detailed understanding of the excitation of cometary C_2 is required in order to extract carbon isotope abundance ratios from observable line intensities (Stawikowski and Greenstein 1964; Owen 1973; Danks, Lambert, and Arpigny 1974; Lambert and Danks 1983). In broader cosmogonical terms, it is important to know whether comets—as likely representatives of primitive solar system material—have isotope abundances more like those of the interstellar medium or like those of the inner solar system. Ultimately, the accuracy

of a spectroscopic determination of the carbon isotope ratio will be limited by the accuracy with which the spectra can be simulated theoretically in order to establish a relation between line intensity and number of emitting molecules. The problem of the excitation of $^{12}C\,^{13}C$ in comets will be considered in detail in Paper II (Gredel, van Dishoeck, and Black 1989), where theoretical profiles will be compared with new high-resolution observations in comet Halley (Wehinger *et al.* 1986).

The model that we adopt for $^{12}C_2$ is presented in § II, and the employed molecular parameters are discussed. In addition, a theoretical estimate of the two intercombination transition moments is undertaken. The results of the calculations are presented in § III. From the theoretical population densities in the various rotational levels, flux ratios and synthetic emission profiles are calculated as functions of the $a\,^3\Pi_u$–$X\,^1\Sigma_g^+$ and the $c\,^3\Sigma_u^+$–$X\,^3\Sigma_g^+$ intercombination transition moments. The influence of each of these two transitions separately on the vibrational and rotational excitation temperatures is investigated. The observed emission spectra of the (0, 0) Swan band in comet Halley are presented § IV, where they are compared to the synthetic profiles.

II. THE MODEL

In the present calculations, stimulated absorption and emission and spontaneous emission processes were included for allowed electronic transitions in the Phillips $A\,^1\Pi_u$–$X\,^1\Sigma_g^+$, Swan $d\,^3\Pi_g$–$a\,^3\Pi_u$, Ballik-Ramsay $b\,^3\Sigma_g^-$–$a\,^3\Pi_u$, and the $d\,^3\Pi_g$–$c\,^3\Sigma_u^+$ systems. In addition, the spin forbidden $a\,^3\Pi_u$–$X\,^1\Sigma_g^+$ and $c\,^3\Sigma_u^+$–$X\,^1\Sigma_g^+$ transitions were considered. The symmetry forbidden $c\,^3\Sigma_u^+$–$b\,^3\Sigma_g^-$ transition is predicted to be much slower (Klotz 1987), and it was neglected. Higher lying states, such as the $D\,^1\Sigma_u^+$ and $e\,^3\Pi_u$ states, have been shown to have negligible influence on the populations in the lower states (Krishna Swamy and O'Dell 1977, 1981, 1987), and were therefore not taken into account. There is an additional $2\,^1\Sigma^+$ state which is shown by theoretical calculations to lie $\sim$2.4 eV above the $X\,^1\Sigma_g^+$ state (Kirby and Liu 1979; van Dishoeck 1983). However, this state is expected to have little effect on the populations in other states, since the only link to the other electronic states considered in this model is an allowed radiative transition to the $A\,^1\Pi_u$ state. An excited rotational level in $A\,^1\Pi_u$ is more likely to decay to the $X\,^1\Sigma_g^+$ state than to undergo an additional excitation to the $2\,^1\Sigma^+$ state. The $2\,^1\Sigma^+$ state was therefore neglected as well. For the triplet states, the three electronic spin-substates were treated explicitly. Sixty rotational levels in each of the six lowest vibrational levels were included in the calculations, resulting in transitions among a total of more than 4000 individual vibration-rotation levels. The excitation energies of the vibrational levels involved in the calculation are presented in the term diagram in Figure 1. The number of vibrational and rotational levels included in the model is adequate to describe the population distributions in the lower vibrational levels $v = 0$–4 for comparison with high-resolution data, which is the primary goal of this work. However, it is insufficient to predict accurate fluxes in entire band sequences.

The model assumes that the level populations are in statistical equilibrium and that resonance fluorescence in the solar radiation field and intercombination transitions are the only mechanisms that determine the population densities of the various levels. In particular, collisional processes in the lower states are neglected, and the C_2 formation process is assumed to have no persistent effects on the level populations. As discussed by Arpigny (1965) and Lambert and Danks (1983), these assumptions appear to be justified because the C_2 excitation rate in the solar radiation field is orders of magnitude more rapid than the formation or collisional rates. The details of the model are discussed in the following three sections.

a) *Absorption and Emission Rates*

It is useful to review briefly the definition of rotational levels and rotational lines for diatomic molecules. Following the notation introduced by Whiting (1973), electronic states split into $2S + 1$ spin substates and, if $\Lambda \neq 0$, into two lambda substates, resulting in a total number of $(2 - \delta_{0,\Lambda})(2S + 1)$ electronic substates for each rotational level characterized by N, J, and p. Here Λ is the component of the electronic orbital angular momentum along the internuclear axis, S is the quantum number of the total electronic spin, N is the angular momentum quantum number excluding electron spin, J denotes the total angular momentum quantum number excluding nuclear spin, and p is the parity, which distinguishes the lambda substates. The electronic substates contain the vibrational and rotational levels, and a rotational line is defined as a transition between two rotational levels. This definition implies that a rotational lambda doublet consists of two rotational lines. Note that $^{12}C_2$ is a homonuclear molecule with zero nuclear spin, so that all antisymmetric rotational levels are missing. Specifically, all odd-J levels are absent in the $X\,^1\Sigma_g^+$ state, whereas half the Λ-doublet levels are not present in the $^1\Pi$ and $^3\Pi$ states.

In the case of an allowed transition between an upper rotational level $v'J'N'p'$ and a lower level $v''J''N''p''$, the spontaneous emission probability $A_{v'J',\,v''J''}$ is related to the band absorption oscillator strength $f_{v'v''}$ according to

$$A_{v'J',\,v''J''} = \frac{8\pi^2 e^2}{mc}\,\tilde{\nu}^2\,\frac{2 - \delta_{0,\Lambda''}}{2 - \delta_{0,\Lambda'+\Lambda''}}\,f_{v'v''}\,\frac{\mathcal{S}_{J'J''}}{2J' + 1} \tag{1}$$

$$= \frac{2 - \delta_{0,\Lambda'}}{2 - \delta_{0,\Lambda'+\Lambda''}}\,A_{v'v''}\,\frac{\mathcal{S}_{J'J''}}{2J' + 1}\ \mathrm{s}^{-1} \tag{2}$$

where $\tilde{\nu} = \nu/c$ is the wavenumber of the transition (Larsson 1983). The Hönl-London or line intensity factors $\mathcal{S}_{J'J''}$ occurring in the above expressions determine the strength of a rotational line. The Hönl-London factors follow sum rules, which have been discussed extensively in the literature, e.g., by Whiting and Nichols (1974), Whiting *et al.* (1980), and Schadee (1975, 1978). The appropriate sum rule for this specific case is

$$\sum_J \mathcal{S}_{J'J''} = N_{D_e} \times (2J + 1)\,, \tag{3}$$

where N_{D_e} is the number of independent transition moments occurring in the transition, $N_{D_e} = (2 - \delta_{0,\Lambda'+\Lambda''})(2S + 1)$, and J may be either J' or J''.

The band oscillator strength $f_{v'v''}$ is related to the electric dipole transition moment $D_e(R)$ (in atomic units)[3] through

$$f_{v'v''} = \frac{2}{3}\,\frac{(2 - \delta_{0,\Lambda'+\Lambda''})}{(2 - \delta_{0,\Lambda''})}\,E_{v'v''}\,|[\chi_{v'}(R)\,|\,D_e(R)\,|\,\chi_{v''}(R)]|^2\,, \tag{4}$$

where χ_v is the vibrational wave function, R is the internuclear distance, $E_{v'v''}$ is the transition energy in atomic units, and the brackets denote that the integration of the matrix element is over R. In the Franck-Condon approximation, the dependence

[3] Note that D_e is equal to R_e in the notation of Whiting and Nicholls (1974).

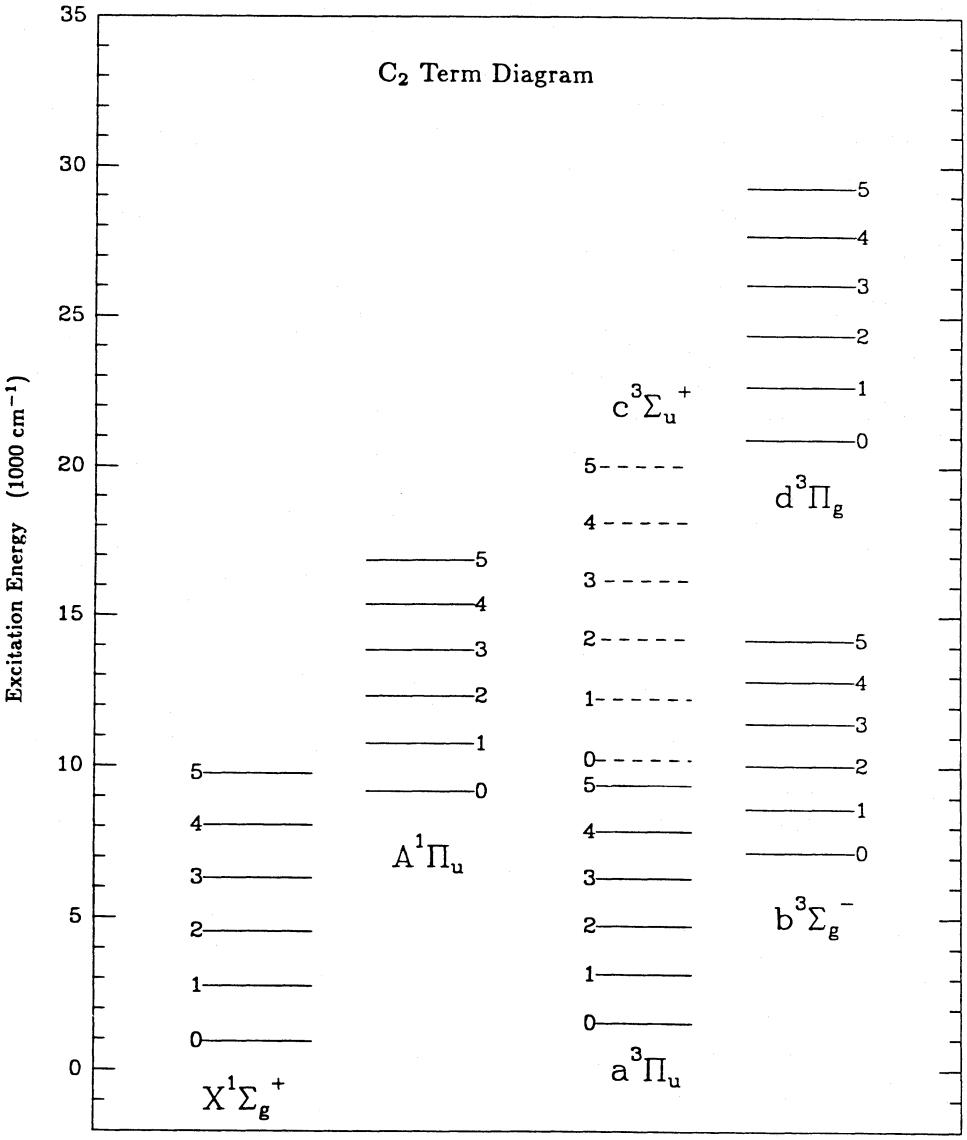

FIG. 1.—C_2 energy level diagram illustrating the electronic states included in this work. The six lowest vibrational levels in each electronic state are indicated. The positions of vibrational levels in the $c\,^2\Sigma_u^+$ state are presented by dashed lines.

of $f_{v'v''}$ on the states involved is assumed to be dominated by the amount of constructive/destructive interference of the vibrational wave functions. Thus

$$f_{v'v''} = \frac{2}{3}\frac{(2-\delta_{0,\Lambda'+\Lambda''})}{(2-\delta_{0,\Lambda''})} E_{v'v''} q_{v'v''} |D_e(R_{eq})|^2 \qquad (5)$$

where

$$q_{v'v''} = |[\chi_{v'}(R)|\chi_{v''}(R)]|^2 \qquad (6)$$

is the Franck-Condon factor, and $D_e(R)$ is replaced by its value at some particular $R = R_{v'v''}$. In many real cases, the R-centroid, $R_{v'v''}$, is a slightly and smoothly varying function of v' and v'', and, when detailed information is lacking, $D_e(R) = D_e(R_{eq})$ is assumed to be constant and equal to its value at the equilibrium internuclear distance, R_{eq}. In what follows, we will use the expression "transition moment" loosely to stand for the proper square of the transition moment when discussing intensities.

The absorption rates $B^{abs}_{v'J',v''J''}\rho_\nu$ and the stimulated emission rates $B^{em}_{v'J',v''J''}\rho_\nu$ follow the relations

$$B^{abs}_{v'J',v''J''}\rho_\nu = \frac{10^7}{8\pi hc^2}\tilde{\nu}^{-5}\frac{(2J'+1)}{(2J''+1)} A_{v'J',v''J''} H_\lambda \left(\frac{1}{\mathscr{R}_c}\right)^2 \text{ s}^{-1}, \qquad (7)$$

$$B^{em}_{v'J',v''J''}\rho_\nu = \frac{(2J''+1)}{(2J'+1)} B^{abs}_{v'J',v''J''}\rho_\nu \text{ s}^{-1}, \qquad (8)$$

where $\rho_\nu = 10^7 H_\lambda/(c\tilde{\nu}^2)$ is the received solar flux in units of ergs cm^{-2} s^{-1} Hz^{-1} and H_λ is the solar irradiance in ergs cm^{-2} s^{-1} nm^{-1} at one astronomical unit (AU). For the wavelength region 2960–13,000 Å the data provided by the high-resolution solar flux atlas of Kurucz *et al.* (1984) were adopted, and for $\lambda > 1.3$ μm the integrated values

$$H^{int}(\lambda) = \int_\lambda^{\lambda+\delta\lambda} H_{\lambda'}\, d\lambda'$$

given by Labs and Neckel (1970) were used to determine the solar irradiance $H_\lambda = H^{\rm int}(\lambda)/\delta\lambda$. The solar flux at an arbitrary heliocentric distance $\mathscr{R}_c$ was obtained by scaling H_λ with the factor $(1/\mathscr{R}_c)^2$ with $\mathscr{R}_c$ in AU.

b) Adopted Molecular Constants

The oscillator strengths for the Phillips $A\,^1\Pi_u$–$X\,^1\Sigma_g^+$ system have recently been reinvestigated by a number of experimental and theoretical techniques. The new studies have significantly reduced the uncertainties that resulted from previous determinations. From radiative lifetime measurements of the $A\,^1\Pi_u$ state vibrational levels, Bauer *et al.* (1985) inferred $f_{00}^{\rm Phillips} = 1.4 \times 10^{-3}$, a value which is consistent with their deduced $f_{00}^{\rm Phillips} = 1.5 \times 10^{-3}$ from laser-induced fluorescence measurements (Bauer *et al.* 1986). Davis *et al.* (1984) found $f_{00}^{\rm Swan}/f_{00}^{\rm Phillips} = 18.2$ from absorption line strength measurements, which gives $f_{00}^{\rm Phillips} = 1.8 \times 10^{-3}$ if the (0, 0) Swan band absorption oscillator strength $f_{00}^{\rm Swan} = 3.2 \times 10^{-2}$ obtained by Stark and Davis (1985) is adopted, and $f_{00}^{\rm Phillips} = 1.6 \times 10^{-3}$ if $f_{00}^{\rm Swan} = 2.9 \times 10^{-2}$ of Bauer *et al.* (1986) is used. The experimental values are smaller by up to a factor of 2 than the earlier theoretical work, which gave $f_{00}^{\rm Phillips} = (2.7 \pm 0.2) \times 10^{-3}$ (van Dishoeck 1983; Chabalowski, Peyerimhoff, and Buenker 1983; Pouilly *et al.* 1983). However, recent more extensive calculations by Klotz (1987) and ONeil, Rosmus, and Werner (1987) suggest lower values, $f_{00}^{\rm Phillips} \approx (2.1\text{–}2.2) \times 10^{-3}$. The remaining small discrepancies between theory and experiment are not yet fully understood. Unfortunately, most of the calculations were performed before the more recent evidence in favor of the lower values became available, and still used the older theoretical oscillator strengths of van Dishoeck (1983). In order to investigate the sensitivity of the computations to the adopted values, results obtained with the experimental oscillator strengths of Bauer *et al.* (1985, 1986) are presented as well. As will be shown below, the effects are small compared with the uncertainties in other crucial parameters.

Transition frequencies in the Phillips system were calculated using the molecular parameters provided by Chauville, Maillard, and Mantz (1977). The Hönl-London factors for the R, Q, and P lines are given by the expressions $J'' + 2$, $2J'' + 1$, and $J'' - 1$, respectively, and satisfy the sum rule $\sum_{J'} \mathscr{S}_{J'J''} = 2(2J'' + 1)$.

For the Swan System, the electric transition dipole moment function $D_e(R)$ varies strongly with internuclear distance R. The theoretical ab initio calculations of Chabalowski, Buenker, and Peyerimhoff (1981) are in good agreement with the experimental findings by Tatarczyk, Fink, and Becker (1976), and with the recent accurate determination by Stark and Davis (1985). We recalculated the Swan band transition probabilities $A_{v'v''}$ explicitly, using the expression

$$A_{v'v''} = 2.026 \times 10^{-6}\, \frac{2 - \delta_{0,\Lambda'+\Lambda''}}{2 - \delta_{0,\Lambda'}}\, \tilde{\nu}^3\, |[\chi_{v'}|D_e(R)|\chi_{v''}]|^2 \ {\rm s}^{-1} . \quad (9)$$

The vibrational eigenfunctions χ_v in the upper and lower electronic states were obtained from a numerical solution of the Schrödinger equation through use of a Numerov procedure. Rydberg-Klein-Rees (RKR) potentials based on the constants of Phillips (1968) were used for the $a\,^3\Pi_u$ and $d\,^3\Pi_g$ states. The dependence of D_e on R has been taken from Chabalowski *et al.* (1981). The results are presented in Table 1. The corresponding lifetime $\tau_{v'} = 1/(\sum_{v''} A_{v'v''})$ is 93 ns for $v' = 0$. This is consistent with the value of 92 ± 5 ns measured by Stark and Davis (1985), if the transition to the $a\,^3\Pi_u$ state is the principal decay channel of the $d\,^3\Pi_g$ state.

TABLE 1

COMPUTED BAND TRANSITION PROBABILITIES[a] $A_{v'v''}$ FOR THE C_2 SWAN $d\,^3\Pi_g$–$a\,^3\Pi_u$ SYSTEM[b]

	v'					
v''	0	1	2	3	4	5
0.....	8.10 (6)	2.96 (6)	3.15 (5)	5.15 (3)	1.02 (3)	2.05 (2)
1.....	2.20 (6)	3.72 (6)	4.31 (6)	6.78 (5)	6.10 (3)	5.33 (3)
2.....	3.85 (5)	2.91 (6)	1.36 (6)	4.64 (6)	9.49 (5)	2.15 (3)
3.....	5.67 (4)	8.46 (5)	2.76 (6)	3.21 (5)	4.48 (6)	1.06 (6)
4.....	7.58 (3)	1.76 (5)	1.21 (6)	2.18 (6)	1.39 (4)	4.14 (6)
5.....	9.51 (2)	3.19 (4)	3.30 (5)	1.38 (6)	1.53 (6)	4.49 (4)

[a] In s^{-1}.

[b] Obtained from theoretical calculations from RKR potentials for the $a\,^3\Pi_u$ and $d\,^3\Pi_g$ states, and the theoretical transition dipole moment function of Chabalowski *et al.* 1981.

Rotational energies in the $a\,^3\Pi_u$ and $d\,^3\Pi_g$ states were calculated using the molecular parameters given by Phillips (1968). For the (0, 0) band, the explicit vacuum wavenumbers tabulated by Amiot (1983) were adopted. The Hönl-London factors were calculated using the expressions tabulated by Kovács (1969), taking into account the corrections to the analytic formulae as provided by Whiting *et al.* (1973). The summation of the Hönl-London factors of all rotational lines involving the symmetric levels with a common J'' yields

$$\sum_{J'} \mathscr{S}_{J'J''} = 3(2J'' + 1) .$$

For the first rotational levels with $J'' < 3$, the numerical values obtained from the computer code by Whiting (1973) were used.

For the Ballik-Ramsay $b\,^3\Sigma_g^-$–$a\,^3\Pi_u$ system, the band transition probabilities calculated by Chabalowski, Peyerimhoff, and Buenker (1983) were used. No recent accurate measurements of the Ballik-Ramsay system exist, but the calculations are consistent with the older shock tube measurements by Cooper and Nicholls (1975). Transition frequencies were calculated using the molecular parameters determined by Roux *et al.* (1985).

Accurate transition frequencies for the $d\,^3\Pi_g$–$c\,^3\Sigma_u^+$ transition are not yet available, although the presence of the $c\,^3\Sigma_u^+$ state appears well established from perturbations of the $v' = 4$, $J' = 52$, 57, and 67, $v' = 5$, $J' = 38$, 43, and 48, and $v' = 6$, $J' = 18$, 23, and 28 levels in the $a\,^3\Pi_u$ state. Rotational energies of the $c\,^3\Sigma_u^+$ state were calculated using molecular parameters derived by Chauville, Maillard, and Mantz (1977). The inverse lifetime of the $d\,^3\Pi_g$ state due to transitions to the $c\,^3\Sigma_u^+$ state can be estimated (see Lambert and Danks 1983) by comparison of accurate lifetime measurements (Stark and Davis 1985) of the Swan system with theoretical determinations of band absorption oscillator strengths (Chabalowski *et al.* 1981), taking the possible errors in both determinations into account. This estimate gives an upper limit on the $d\,^3\Pi_g$–$c\,^3\Sigma_u^+$ decay rate of 10% of the $d\,^3\Pi_g$–$a\,^3\Pi_u$ inverse lifetime. If, on the other hand, the transition moments of the $d\,^3\Pi_g$–$c\,^3\Sigma_u^+$ system were as large as those of the Swan system, the inverse radiative lifetime for the d–c transition would be given by $A_{00}^{d-c} = (\tilde{\nu}_{00}^{d-c}/\tilde{\nu}_{00}^{\rm Swan})^3 \times A_{00}^{d-a} \approx 0.19 A_{00}^{d-a}$. Preliminary results from ab initio calculations (Klotz 1987) indicate that the $d\,^3\Pi_g$–$c\,^3\Sigma_u^+$ transition moment is about a factor of 3 smaller than the

$d\,^3\Pi_g$–$a\,^3\Pi_u$ transition moment at $R_{eq} = 2.36$ bohr. If both transition moments had a similar dependence on the internuclear separation, the d–c transition would amount to ~2% of the total decay rate of the d vibrational levels. If, however, the $d\,^3\Pi_g$–$c\,^3\Sigma_u^+$ transition moment were constant in the Franck-Condon regime, the contribution of the $d\,^3\Pi_g$–$c\,^3\Sigma_u^+$ transitions to the total decay rate of $d\,^3\Pi_g$ would be higher than 2%. Most of the present calculations were performed before the theoretical estimate of the $d\,^3\Pi_g$–$c\,^3\Sigma_u^+$ transition moment by Klotz (1987) became available. In most calculations therefore, a constant ratio of $A^{d-c}_{v'v''}/A^{\text{Swan}}_{v'v''} = 0.1$ was used, but results obtained with values as small as 0.01 are presented as well in § III. In the absence of the $c\,^3\Sigma_u^+$–$X\,^1\Sigma_g^+$ intercombination transition, the strength of the $d\,^3\Pi_g$–$c\,^3\Sigma_u^+$ transition would not be important, since in this case the population density in the $c\,^3\Sigma_u^+$ levels would be exclusively determined by the ratio of the Einstein coefficients for absorption, and emission and the transition moment would factor out. The $c\,^3\Sigma_u^+$ state cannot decay by allowed electronic transitions to any of the lower lying triplet states. Without the $c\,^3\Sigma_u^+$–$X\,^1\Sigma_g^+$ intercombination transition, the total population density residing in the $c\,^3\Sigma_u^+$ state would be ~10% of that in the $a\,^3\Pi_u$ state.

For all allowed electronic transitions discussed above, the rotational dependence of the vibrational wave functions has been neglected. Dwivedi *et al.* (1978) have shown for most of these transitions that the variation of the Franck-Condon factors with increasing J is at most a few percent up to $J = 60$.

c) *Intercombination Transitions*

The lifetimes of rotational levels due to intercombination transitions were calculated according to the expression

$$A_{v'J',v''J''} = \frac{64\pi^4}{3h}\,\tilde{\nu}^3\,\frac{\sum_{N_{De}} |D_e|^2}{N_{D_e}}\,q_{v'v''}\,\frac{\mathcal{S}_{J'J''}}{2J'+1}\,. \qquad (10)$$

The line intensity factors $\mathcal{S}_{J'J''}$ follow the sum rule as given by equation (3). For the $c\,^3\Sigma_u^+$–$X\,^1\Sigma_g^+$ transition, $N_{D_e} = 1$ and $\mathcal{S}_{J'J''} = J/2, (J+2)/2, (J-1)/2$, and $(J+1)/2$ for the ^RQ, R, P, and ^PQ lines, respectively. In the $a\,^3\Pi_u$–$X\,\Sigma_g^+$ system, two independent transition moments occur; the line intensity factors were calculated with the analytic expressions of Kovács (1969).

A theoretical estimate of the intercombination transition moments was undertaken extending the discussion presented by Lambert and Danks (1983). Spin forbidden electric dipole transitions can occur between perturbed singlet and triplet states. In the case of the $a\,^3\Pi_u$–$X\,^1\Sigma_g^+$ intercombination transition in C_2, the spin-orbit interaction causes a mixing of the $a\,^3\Pi_u$ wave functions with the $A\,^1\Pi_u$ wave functions. Because of the small singlet character of the $a\,^3\Pi_u$ eigenfunctions, the matrix element of the dipole moment operator between the $a\,^3\Pi_u$ and $X\,^1\Sigma_g^+$ wave functions is no longer zero. In second-order perturbation theory, the wave functions $\Psi_{e,v}$ of electronic-vibrational state e, v are conveniently written in terms of

$$|e, v\rangle = |e, v\rangle_0 + \sum_{e'}\sum_{v'} |e', v'\rangle_0\,\frac{\langle e', v'|\mathcal{H}_{\text{so}}|e, v\rangle_0}{(E_{e',v'} - E_{e,v})}\,, \qquad (11)$$

where the summation is extended over the unperturbed basis functions of electronic and vibrational states $|e, v\rangle_0$. In their estimate, Lambert and Danks (1983) considered the contribution of the $A\,^1\Pi_u$ state to the $a\,^3\Pi_u$ wave function. They obtained a value for the intercombination transition-moment squared of $|D_{a-X}|^2 \approx 10^{-7}$ a.u., much lower than the value of $|D_{a-X}|^2 \approx 10^{-5}$ a.u. required by the theoretical models to bring the observed cometary flux ratios into agreement with the predictions, leading them to conjecture that additional mixings are present in C_2. In particular, Cooper (as cited in Lambert and Danks 1983) had pointed out that the mixing of the $X\,^1\Sigma_g^+$ state with the $b\,^3\Sigma_g^-$ state further facilitates the $a\,^3\Pi_u$–$X\,^1\Sigma_g^+$ intercombination transition. Note that the latter mixing does not mean that the $b\,^3\Sigma_g^-$–$X\,^1\Sigma_g^+$ intercombination transition occurs as an electric dipole transition, as was apparently assumed by Krishna Swamy and O'Dell (1987).

In a rigorous theoretical calculation of rotational lifetimes for the $a\,^3\Pi_u$–$X\,^1\Sigma_g^+$ intercombination transition, Le Bourlot and Roueff (1986) considered both the $a\,^3\Pi_u$–$A\,^1\Pi_u$ and the $X\,^1\Sigma_g^+$–$b\,^3\Sigma_g^-$ mixing. They obtained the wave functions of the individual vibration-rotation levels of the electronic states by diagonalizing the Hamiltonian matrix, which included all rotational dependences of the perturbations. The lifetimes of the lowest 30 rotational levels in the lowest 14 vibrational states in both the $X\,^1\Sigma_g^+$ and a $a\,^3\Pi_u$ states due to intercombination transitions were calculated, and a decrease of the rotational lifetimes by about a factor of 2 was found after inclusion of the $X\,^1\Sigma_g^+$–$b\,^3\Sigma_g^-$ mixing.

Klotz (1987) has recently performed a very detailed calculation of the spin-orbit matrix elements between the various electronic states of C_2. From his calculations it appears that the $X\,^1\Sigma_g^+$ state mixes not only with the $b\,^3\Sigma_g^-$ state but also with the $d\,^3\Pi_g$ state. The $X\,^1\Sigma_g^+$–$d\,^3\Pi_g$ mixing may contribute since the $a\,^3\Pi_u$–$X\,^1\Sigma_g^+$ intercombination transition then "steals" intensity from the strong $d\,^3\Pi_g$–$a\,^3\Pi_u$ transition. Furthermore, the $A\,^1\Pi_u$ state mixes both with the $a\,^3\Pi_u$ and the $c\,^3\Sigma_u^+$ states, and in addition the $c\,^3\Sigma_u^+$ state mixes with the $a\,^3\Pi_u$ state.

The $a\,^3\Pi_u$–$X\,^1\Sigma_g^+$ and the $c\,^3\Sigma_u^+$–$X\,^1\Sigma_g^+$ intercombination transition moments were calculated with adoption of the spin-orbit matrix elements between electronic wave functions kindly provided by Klotz (1987). For instance, the following expression is obtained for the matrix element of the electric dipole moment operator $\boldsymbol{d}$ between the $a\,^3\Pi_u$ and $X\,^1\Sigma_g^+$ states:

$$\begin{aligned}\langle X, v_1|\boldsymbol{d}|a, v_2\rangle = \sum_{v'}\Bigg\{&\langle X, v_1|\boldsymbol{d}|A, v'\rangle\,\frac{\langle A, v'|\mathcal{H}_{\text{so}}|a, v_2\rangle}{(E_{A,v'} - E_{a,v_2})}\\ &+ \langle b, v'|\boldsymbol{d}|a, v_2\rangle\,\frac{\langle b, v'|\mathcal{H}_{\text{so}}|X, v_1\rangle}{(E_{b,v'} - E_{X,v_1})}\\ &+ \langle d, v'|\boldsymbol{d}|a, v_2\rangle\,\frac{\langle d, v'|\mathcal{H}_{\text{so}}|X, v_1\rangle}{(E_{d,v'} - E_{X,v_1})}\Bigg\}\,,\end{aligned} \qquad (12)$$

where the wave functions of the individual electronic states $X\,^1\Sigma_g^+$, $A\,^1\Pi_u$, $a\,^3\Pi_u$, $b\,^3\Sigma_g^-$, $c\,^3\Sigma_u^+$, and $d\,^3\Pi_g$ are indicated by the letters X, A, a, b, c, and d. A similar expression is obtained for the $c\,^3\Sigma_u^+$–$X\,^1\Sigma_g^+$ transition. In the present calculation, the contribution of certain terms was not treated explicitly. For instance, the term $\sum_{v'}\langle c, v_1|\boldsymbol{d}|b, v'\rangle\langle b, v'|\mathcal{H}_{\text{so}}|X, v_2\rangle/(E_{b,v'} - E_{X,v_2})$ in the expression for the $a\,^3\Pi_u$–$X\,^1\Sigma_g^+$ transition was neglected. Both matrix elements would be zero in the absence of the spin-orbit coupling, and their product is a small number. Accordingly, all terms involving similar products were neglected. In the present calculations, 10 vibrational levels in each electronic state were employed, and the inclusion of more vibrational levels turned out not to influence the results

obtained for the six lowest vibrational levels. Note that this formulation does not consider selection rules for individual Ω states, as will be discussed below.

In the Born-Oppenheimer approximation, the integration over the electron coordinates can be separated from the integration over the nuclear coordinates, and the above matrix elements factor into Franck-Condon factors and transition moments, as discussed in § II*a*. The vibrational wave functions for the various states were obtained by solving the Schrödinger equation with a Numerov procedure. The potential curves were created using the empirical RKR method based on the constants of Chauville *et al.* (1977), Phillips (1968), and Roux *et al.* (1985) for the various states. The results for the $|D_{a-X}|^2$ and $|D_{c-X}|^2$ transition moments squared are presented in Table 2 for both the theoretical and the experimental oscillator strengths for the Phillips $A\,^1\Pi_u$–$X\,^1\Sigma_g^+$ transition. Also included in Table 2 are the $a\,^3\Pi_u$–$X\,^1\Sigma_g^+$ transition moments that are obtained if only the $X\,^1\Sigma_g^+$–$b\,^3\Sigma_g^-$ and $A\,^1\Pi_u$–$a\,^3\Pi_u$ mixings are taken into account. It appears that the inclusion of the other couplings increases the $|D_{a-X}|^2$ values by a small fraction.

The lifetimes of the vibrational levels due to intercombination transitions are inversely proportional to the transition moments given in Table 2. Unfortunately, it is much more difficult to treat the rotational dependence adequately. For spin-allowed transitions, the vibrational lifetimes are converted to rotational lifetimes as indicated by equation (2). In the case of intercombination transitions, this treatment cannot be applied, as James (1971) pointed out. The reason is that the perturbation which makes the intercombination transition electric dipole allowed depends on the rotational quantum number J. The $(2 - \delta_{0,\Lambda})(2S + 1)$–fold degeneracy of the vibrational states introduces further complications. Suppose the intercombination transitions are facilitated by the mixing of singlet and triplet wave functions, as is the case for C_2. According to the selection rule, $\Delta\Omega = 0$ for homogeneous perturbations, a $^3\Pi$, $\Omega = 1$ wave function would mix only with a $^1\Pi$ wave function, whereas a $^3\Pi$, $\Omega = 0$ wave function would mix only with one of $^1\Sigma$ type. Accordingly, the lifetimes of rotational states in $^3\Pi$, $\Omega = 2$ would be infinite. For higher rotational quantum numbers, however, the three electronic substrates $\Omega = 0, 1, 2$ mix together as the coupling case eventually reaches Hund's case b. As a result, the lifetimes of rotational levels in $\Omega = 2$ decrease drastically with increasing J.

It is obvious that for intercombination transitions the simple factorization into a transition moment, a Franck-Condon factor and an intensity factor for the lifetime of a rotational state, as indicated by equation (10), has only limited value. In fact, the lifetimes for the individual rotational levels must be calculated separately in order to obtain exact expressions. The proper way to do the calculation was described by Le Bourlot and Roueff (1986). Unfortunately, their calculations were limited to $J \leq 30$, and included only the $X\,^1\Sigma_g^+$–$b\,^3\Sigma_g^-$ and $a\,^3\Pi_u$–$A\,^1\Pi_u$ interactions. It would be desirable to extend their calculations to the higher rotational levels in the $a\,^3\Pi_u$ and $X\,^1\Sigma_g^+$ states, and to the lifetimes of rotational levels in the $c\,^3\Sigma_u^+$–$X\,^1\Sigma_g^+$ intercombination system. An indication of the reliability of the results listed in Table 2 can be obtained by comparing the inverse radiative lifetimes based on the estimated values—with only the $X\,^1\Sigma_g^+$–$b\,^3\Sigma_g^-$ and $a\,^3\Pi_u$–$A\,^1\Pi_u$ couplings included—with the detailed theoretical values listed by Le Bourlot and Roueff (1986). The estimated values agree within factors of 3. As a preliminary test of the sensitivity of the level populations to the detailed values of the transition probabilities, some calculations were performed including the individual rotational-level specific transition probabilities kindly provided by Le Bourlot and Roueff (1986) up to $J = 30$, extended to higher J values by our more approximate treatment.

TABLE 2

THEORETICAL INTERCOMBINATION TRANSITION MOMENTS FOR THE $a\,^3\Pi_u$–$X\,^1\Sigma_g^+$ AND $c\,^3\Sigma_u^+$–$X\,^1\Sigma_g^+$ TRANSITIONS[a,b]

v'' (1)	v' (2)	$\lvert D_{a-X}\rvert^2$ (3)	$\lvert D_{c-X}\rvert^2$ (4)	$\lvert D_{a-X}\rvert^2$ (5)	$\lvert D_{c-X}\rvert^2$ (6)	$\lvert D_{a-X}\rvert^2$ (7)
0	0.....	8.2 (−7)	4.4 (−7)	5.2 (−7)	2.4 (−7)	5.5 (−7)
1[c]	0.....	9.4 (−7)	5.1 (−6)	6.1 (−7)	2.7 (−6)	6.3 (−7)
2[c]	0.....	1.2 (−6)	2.1 (−4)	8.5 (−7)	1.1 (−4)	8.6 (−7)
0	1.....	7.7 (−7)	1.2 (−5)	4.8 (−7)	6.0 (−6)	5.1 (−7)
1	1.....	1.0 (−6)	8.6 (−7)	6.6 (−7)	4.7 (−7)	7.2 (−7)
2[c]	1.....	1.0 (−6)	2.1 (−7)	6.8 (−7)	9.8 (−8)	7.1 (−7)
0	2.....	7.3 (−7)	1.3 (−5)	4.5 (−7)	7.0 (−6)	4.9 (−7)
1	2.....	7.9 (−7)	2.0 (−6)	4.9 (−7)	1.0 (−6)	5.3 (−7)
2	2.....	7.5 (−7)	6.0 (−8)	4.6 (−7)	3.7 (−8)	4.9 (−7)

NOTES.—Cols. (3) and (4) were obtained using the theoretical oscillator strengths of van Dishoeck 1983 for the Phillips system Cols. (5) and (6) were obtained using the experimental oscillator strengths of Bauer *et al.* (1985) for the Phillips $A\,^1\Pi_u$–$X\,^1\Sigma_g^+$ system. Col. (7) was obtained including only the $a\,^3\Pi_u$–$A\,^1\Pi_u$ and $X\,^1\Sigma_g^+$–$b\,^3\Sigma_g^-$ couplings, using the theoretical oscillator strengths for the Phillips system.

[a] All transition moments are in atomic units.

[b] Obtained from second-order perturbation theory (see § II*c* and eq. [12]).

[c] The $X\,^1\Sigma_g^+$ level is the upper state in the a–X transition. In all other cases, the $a\,^3\Pi_u$ or $c\,^3\Sigma_u^+$ levels are the upper states.

d) Synthetic Spectra

The population densities in the various vibration-rotation levels of the singlet and triplet states are determined by a set of steady state rate equations containing the transition probabilities discussed in the previous sections. However, the solution of the more than 4000 linear equations cannot be achieved through standard elimination techniques, and an approximation had to be applied in order to solve the equation system. The employed procedure is discussed in the Appendix, and consists of neglecting all satellite branches with $\Delta J \neq \Delta N$ in the triplet transitions, because of their relative weakness. In particular, for the Swan system only the P_i, Q_i, and R_i lines with $i = 1$–3 were included.

Given the total column density of C_2 molecules $N(C_2)$ and the relative population densities in the various energy levels, the column density $N(v'J')$ (in cm^{-2}) in an excited vibration-rotation level $v'J'N'p'$ can be determined. The integrated intensity I_0 emitted by a $v'J' \rightarrow v''J''$ rotational line at wavelength λ_0 into 4π sr is given by

$$4\pi I_0 = N(v'J')A_{v'J',v''J''}\,hc/\lambda_0 \text{ ergs s}^{-1}\text{ cm}^{-2}\,. \qquad (13)$$

The intrinsic widths, $\delta\lambda$, of cometary emission lines are expected to be $c\,\delta\lambda/\lambda_0 \approx 1$ km s^{-1} or less, so that the dominant broadening will tend to be instrumental. The integrated intensity has therefore been convolved with a Gaussian line shape with a width corresponding to the instrumental response. The synthetic profile is obtained by carrying out the summation of the contributing intensities of the rotational lines in the wavelength region considered.

III. RESULTS

a) Intensity Alternation in the Swan Bands

As a test of the accuracy of the calculations, the excitation of C_2 by an undiluted blackbody radiation field characterized by

a temperature of 5800 K has been computed. In this case the population density of all rotational levels in ground and excited states should follow a thermal distribution characterized by 5800 K. For all reasonable values of the strength of the intercombination transition moments, the deviations of the excitation temperatures from the expected value of 5800 K were found to be less than 0.5%.

A second test has been performed for a blackbody radiation field at $T = 5800$ K, but with a dilution factor $W = 0.25(R_\odot/\mathscr{R}_c)^2$ of 5.42×10^{-6}, a value equal to the dilution of the solar radiation field at 1 AU. Again a blackbody radiation field was employed instead of the solar radiation field in order to demonstrate the effects introduced by the intercombination transitions. The solar radiation field would introduce a secondary effect, namely a partial decrease of the population density in rotational levels in the $d\,^3\Pi_g$ state for which the corresponding rotational transitions coincide with absorption lines in the solar spectrum.

A significant decrease of the vibrational and rotational excitation temperatures characterizing the level populations was found from 5800 K to about 4000 K for $|D_{a-X}|^2 = 10^{-4}$ a.u. A quantitative discussion of the dependence of the population distribution on the values of the intercombination transition moments will be presented in the following section. In this section, the discussion is aimed at another effect that is introduced by the intercombination transitions. In Figures 2*a*–2*c* and 2*d*–2*f* the rotational level populations $n(J)$ in the $v' = 0$ state of the three electronic substates in $d\,^3\Pi_g$ are presented for intercombination transition moments of $|D_{a-X}|^2 = 5 \times 10^{-5}$ and 10^{-4} a.u., respectively. These values are considerably higher than the estimates presented in Table 2, but were chosen to maximize the effects. The $c\,^3\Sigma_u^+$ state was not taken into account in these tests. The first thing to notice is that a systematic population difference occurs between the even and odd rotational levels in all three $a\,^3\Pi_u$ substates, in the sense that the population density of the even N levels in the three electronic sublevels is enhanced with respect to the two adjacent levels $N - 1$ and $N + 1$. Since in the $d\,^3\Pi_g$–$a\,^3\Pi_u$ system only lines with $\Delta N = \Delta J = +1$ occur strongly, the even N levels in the $d\,^3\Pi_g$ substates are overpopulated as well (see figures). This effect must of course not be confused with the alternation of the population density in symmetric and antisymmetric rotational levels in the case of molecules with nonzero nuclear spin, which results from the fact that the respective levels have different statistical weights. Second, it is evident that the three electronic substates have a different population distribution among the rotational levels. This effect is introduced by the intercombination transitions and has its origins in differences in the line intensity factors for the three intercombination subtransitions, thereby demonstrating the importance of treating the three spin components of the triplet states separately.

If the rotational populations in each of the $d\,^3\Pi_g$ $v' = 0$ substates were relaxed to a single rotational temperature $T_{\rm rot}$, the values of $-\ln [n(J)/(2J + 1)]$ versus energy $E(J)hc/k$ (in K) should lie on a line with slope $1/T_{\rm rot}$. Figures 2*a*–2*f* illustrate that the population distribution is nonthermal, even for $|D_{a-X}|^2 \approx 10^{-5}$ a.u., and that both the deviation from a thermal population and the population difference between even and odd rotational states increase with larger $|D_{a-X}|^2$. The straight line drawn in Figure 2 represents a least-squares fit to the data taking all rotational levels into account, and the corresponding rotational temperature is indicated in the upper right-hand corner of each figure. If only levels with $J > 20$ are considered, the rotational temperatures may be lower by as much as 1000 K. The rotational temperatures in higher v are similar to those found in $v = 0$ within a few hundred degrees.

Since the intensity of the emission lines is proportional to the population density of the upper rotational levels, an intensity alternation in the emission spectrum is predicted, the magnitude of which will depend on the strength of the $a\,^3\Pi_u$–$X\,^1\Sigma_g^+$ intercombination transition. The effect is due to transitions to the $X\,^1\Sigma_g^+$ state, where all odd-numbered rotational levels are missing. Note, however, that the alternations are only noticeable for rather high values of the $a\,^3\Pi_u$–$X\,^1\Sigma_g^+$ intercombination transition moment. The effect does not occur when the rotational levels are thermally excited (Phillips 1957).

Some laboratory spectra (Bleekrode and Nieuwpoort 1965) show evidence of intensity alternations in C_2 emission. However, as Nieuwpoort and Bleekrode (1969) explain, these alternations are most likely caused by collision-induced transitions, and do therefore not apply to cometary atmospheres. Lambert and Danks (1983) also found alternations of the peak intensity of the $P_1 + P_2$ blends with N in flame spectra, but attributed the effect to the staggering expected for C_2 lines, i.e., an alternating displacement of the symmetric N Λ-sublevels from a mean position determined if the Λ-splitting were zero. They did not observe an alternation of the equivalent widths of the $P_1 + P_2$ blends. In principle, experimental observations of the intensity alternations for the R_2 lines at low pressures could provide a method for a determination of the $a\,^3\Pi_u$–$X\,^1\Sigma_g^+$ intercombination transition moment, provided that all relevant physical conditions—including the radiation field—could be accurately characterized in the experiments.

If a detailed solar spectrum instead of a blackbody radiation field is employed, the intensity alternations persist. However, Fraunhofer lines in the solar spectrum can affect the populations of individual levels of C_2. Numerous moderately strong Fe I absorption lines in the solar spectrum coincide with cometary emission lines of the Swan (0, 0) band, while the very strong Mg I lines at 5167.327, 5172.698, and 5183.619 Å lie just longward of the C_2 band head.

b) Population Distributions and Synthetic Spectra

In this section, the dependence of the population densities in the various vibration-rotation levels on the strengths of the $a\,^3\Pi_u$–$X\,^1\Sigma_g^+$ and the $c\,^3\Sigma_u^+$–$X\,^1\Sigma_g^+$ intercombination transitions is discussed. In the first part of this section calculations obtained without the $c\,^3\Sigma_u^+$–$X\,^1\Sigma_g^+$ intercombination transitions are presented, and then the modifications introduced by it are discussed. Unless otherwise noted, all calculations used the high-resolution solar flux atlas and values for the heliocentric velocity and distance of the absorbers of $v_c = -26.67$ km s^{-1} and $\mathscr{R}_c = 1.0$ AU, respectively. The heliocentric radial velocity was chosen for comparison with observations of comet Halley, which will be discussed in § IV. Although individual lines may be affected if a different velocity is adopted, the general conclusions are not expected to vary much. The calculations discussed in the following are based on theoretical lifetimes for the Phillips system of van Dishoeck (1983). Results obtained with the experimental values of Bauer *et al.* (1985) are presented at the end of this section.

i) *Effect of the $a\,^3\Pi_u$–$X\,^1\Sigma_g^+$ Transition*

In Table 3, the ratios of the fluxes emitted in various vibrational bands in the singlet and triplet transitions are collected for values of the $a\,^3\Pi_u$–$X\,^1\Sigma_g^+$ intercombination transition

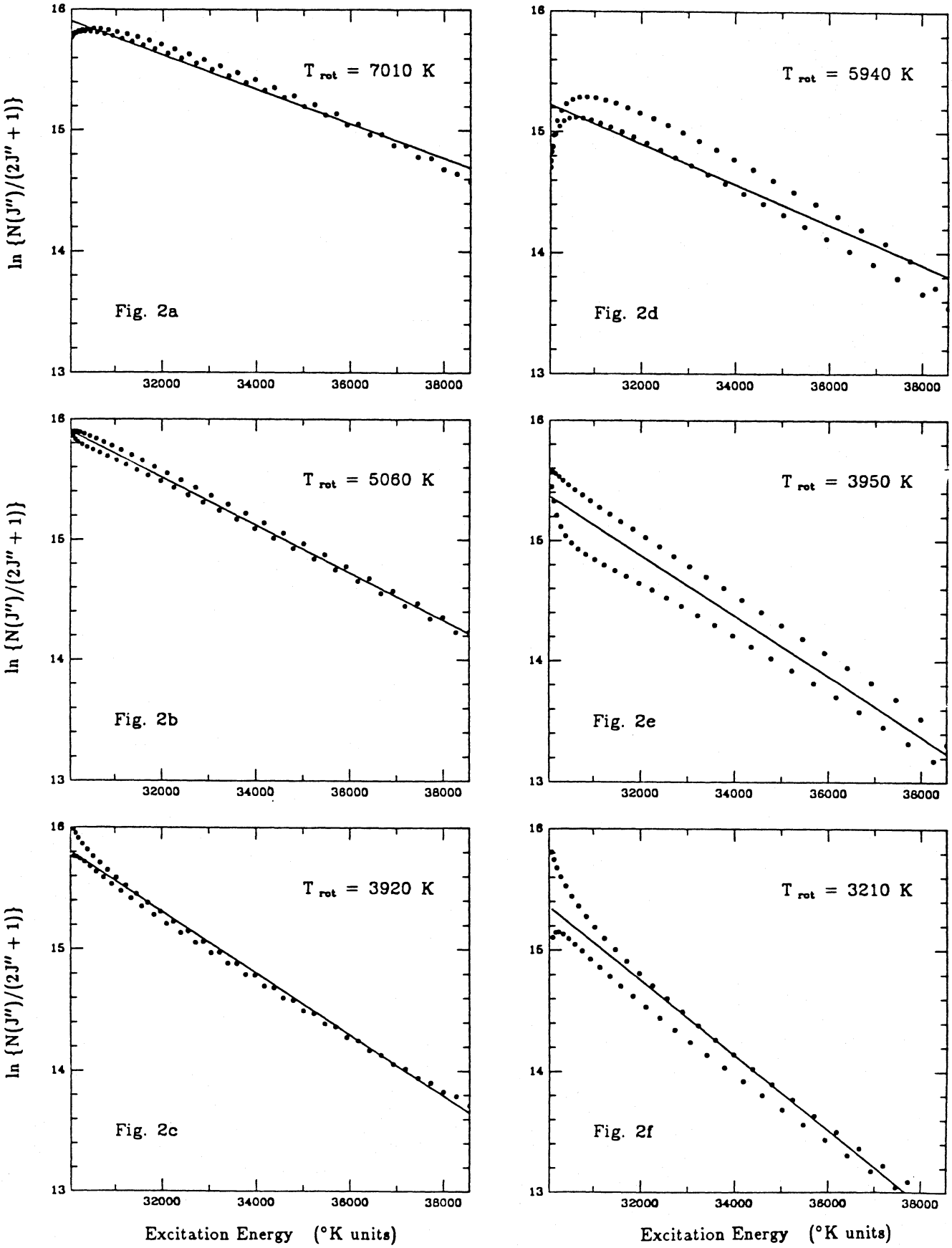

FIG. 2.—The rotational populations in the $v' = 0$ levels of the three spin substates of the $d\,^3\Pi_g$ state. (*a*)–(*c*) The F_1, F_2, and F_3 sublevels, respectively, obtained with a value of the $a\,^3\Pi_u$–$X\,^1\Sigma_g^+$ intercombination transition moment of $|D_{a-X}|^2 = 5 \times 10^{-5}$ a.u. (*d*–*f*) $|D_{a-X}|^2 = 10^{-4}$ a.u. The total C_2 column density is 10^{15} molecules cm^{-2}. Straight line in each figure corresponds to a least-squares fit to all data points. The corresponding rotational temperature is indicated.

TABLE 3

FLUX RATIOS AS FUNCTIONS OF THE $a\,^3\Pi_u$–$X\,^1\Sigma_g^+$ INTERCOMBINATION TRANSITION MOMENT[a,b]

SYSTEMS	$\lvert D_{a-X}\rvert^2$ 10^{-8}	10^{-7}	10^{-6}	10^{-5}	10^{-4}	10^{-3}	c	d
Swan (1, 0)/Swan (0, 0)	2.58 (−1)	2.58 (−1)	2.55 (−1)	2.31 (−1)	1.67 (−1)	1.21 (−1)	2.47 (−1)	2.54 (−1)
Phillips (0, 0)/Swan (0, 0)	4.34 (−2)	4.32 (−2)	6.14 (−2)	1.14 (−1)	1.65 (−1)	2.82 (−1)	1.52 (−1)	5.53 (−2)
Phillips (2, 0)/Swan (0, 0)	2.42 (−2)	2.41 (−2)	2.41 (−2)	5.87 (−2)	7.99 (−2)	1.33 (−1)	8.43 (−2)	2.92 (−2)
Phillips (0, 0)/Ballik-Ramsay (0, 0)	8.25 (−1)	8.21 (−1)	1.17	2.21	3.20	5.38	2.85	1.03
Ballik-Ramsay (0, 0)/Swan (0, 0)	5.26 (−2)	5.26 (−2)	5.24 (−2)	5.16 (−2)	5.15 (−2)	5.24 (−2)	5.33 (−2)	5.35 (−2)
$a\,^3\Pi_u$–$X\,^1\Sigma_g^+$(0, 0)/Swan (0, 0)	2.27 (−8)	2.27 (−7)	2.31 (−6)	2.63 (−5)	3.53 (−4)	4.25 (−3)	1.01 (−6)	1.02 (−5)

[a] $\lvert D_{a-X}\rvert^2$ is in atomic units.
[b] Obtained with $\lvert D_{c-X}\rvert^2 = 0$, and a heliocentric distance and velocity of the absorbers of $\mathscr{R}_c = 1.0$ AU and $v_c = -26.67$ km s^{-1}.
[c] Obtained using the theoretical estimates for the $\lvert D_{a-X}\rvert^2$ transition moment (see § IIc and Table 2).
[d] Obtained using the detailed theoretical line probabilities of Le Bourlot and Roueff 1986 up to $J = 30$ for the $a\,^3\Pi_u$–$X\,^1\Sigma_g^+$ transition, extended to higher J with $\lvert D_{a-X}\rvert^2 = 3.5 \times 10^{-6}$ a.u.

moment ranging from 10^{-8} to 10^{-3} a.u., with $\lvert D_{c-X}\rvert^2 = 0$ adopted throughout. The total fluxes in the vibrational bands were obtained by summing over all rotational lines. Apart from the almost linear increase of the flux in the (0, 0) band of the $a\,^3\Pi_u$–$X\,^1\Sigma_g^+$ transition with $\lvert D_{a-X}\rvert^2$, the most sensitive measure for the strength of the intercombination transition is the ratio of fluxes in singlet transitions with respect to triplet transitions. In the range $10^{-7} < \lvert D_{a-X}\rvert^2 < 10^{-3}$ a.u., the flux emitted in the singlet bands increases by $\sim$50% with each factor of 10 increase in $\lvert D_{a-X}\rvert^2$. The increase of the flux emitted in the singlet bands reflects an increase in the singlet population densities and results from the net effect of both the $a\,^3\Pi_u$–$X\,^1\Sigma_g^+$ and $X\,^1\Sigma_g^+$–$a\,^3\Pi_u$ intercombination transitions which lead to a decay of triplet population density to the $X\,^1\Sigma_g^+$ electronic ground state. The variation of the flux in the Swan (1, 0) band with respect to the flux in the Swan (0, 0) band is less pronounced but manifests itself in the dependence of the (vibrational) excitation temperature of the $d\,^3\Pi_g$ vibrational states on $\lvert D_{a-X}\rvert^2$. The flux emitted in the Ballik-Ramsay (0, 0) band is almost proportional to the flux in the Swan (0, 0) band for the values of $\lvert D_{a-X}\rvert^2$ considered. The flux ratio would be constant if there were no decay of $a\,^3\Pi_u$ population density to the $b\,^3\Sigma_g^-$ state, since both the Swan and the Ballik-Ramsay system share the same lower electronic state. Also included in Table 3 are the flux ratios obtained if the simple theoretical estimate (see § IIc) of the $a\,^3\Pi_u$–$X\,^1\Sigma_g^+$ transition moment is used, as well as the results if the individual rotational line transition probabilities of Le Bourlot and Roueff (1986) are employed up to $J = 30$ and extended to higher J values using a constant $\lvert D_{a-X}\rvert^2 = 3.5 \times 10^{-6}$ a.u. It appears that the theoretical estimate mimics the effects of a mean $\lvert D_{a-X}\rvert^2 \approx 10^{-6}$–$10^{-5}$ a.u. for the Swan band ratios and a higher value, $\lvert D_{a-X}\rvert^2 \approx 10^{-5}$–$10^{-4}$ a.u. for the Swan to Phillips band ratios. Note that these "mean" values are actually higher than each of the individual transition moments listed in Table 2. This results from the fact that the triplet-singlet decays are more efficient than the singlet-triplet transitions, so that relatively more population ends up in the singlet states. The detailed theoretical transition probabilities of Le Bourlot and Roueff (1986) are consistent with a mean $\lvert D_{a-X}\rvert^2 \approx 10^{-6}$ a.u.

In Table 4, the corresponding results are presented as functions of the heliocentric distance $\mathscr{R}_c$ of the absorbers. The two values tabulated for each flux ratio correspond to $\lvert D_{a-X}\rvert^2 = 10^{-5}$ and 10^{-4} a.u. for the upper and lower entry, respectively, and again $\lvert D_{c-X}\rvert^2 = 0$. In general, an increase in heliocentric distance for a fixed value of $\lvert D_{a-X}\rvert^2$ has an effect similar to that of an increase in the value of $\lvert D_{a-X}\rvert^2$ for fixed $\mathscr{R}_c$. With increasing $\mathscr{R}_c$, intercombination transitions compete more effectively with allowed absorptions in depopulating levels of the $a\,^3\Pi_u$ state, and the magnitude of the effect is larger, the larger the value of $\lvert D_{a-X}\rvert^2$. Thus for small $\lvert D_{a-X}\rvert^2 \lesssim 10^{-6}$ a.u., no significant variation of the flux ratios with $\mathscr{R}_c$ is found. The variation is noticeable in the Swan (1, 0)/Swan (0, 0) flux ratio and leads to a decrease of the flux emitted in the (1, 0) band with respect the (0, 0) band emission by $\sim$30% as $\mathscr{R}_c$ increases from 0.5 AU to 2 AU and $\lvert D_{a-X}\rvert^2 \gtrsim 10^{-5}$ a.u. The variation is, however, more pronounced in the singlet to triplet flux ratios. For example, over the same range of $\mathscr{R}_c$, the Phillips (0, 0)/Swan (0, 0) flux ratio almost doubles, and the flux emitted in the (0, 0) intercombination band increases by a factor of 20.

Except for the ratio of fluxes in the Phillips (0, 0) and Ballik-Ramsay (0, 0) bands, the results presented in Table 4 cannot be compared directly with the calculations presented by Krishna Swamy and O'Dell (1987), who tabulated mostly flux ratios for entire band sequences. As discussed before, the number of vibrational levels included in our work is insufficient to obtain fluxes in band sequences accurate to better than $\sim$30%. The close agreement between the Phillips (0, 0)/Ballik-Ramsay (0, 0) flux ratios obtained in the two calculations must be accidental considering the fact that the adopted Phillips system oscillator strengths differ by a factor of 2.

The population distribution among the thousands of levels is most conveniently discussed in terms of rotational and vibrational temperatures. In the following presentation, the mean rotational temperature refers to the population distribution of all rotational levels in a given vibrational state. It was

TABLE 4

FLUX RATIOS AS FUNCTIONS OF HELIOCENTRIC DISTANCE $\mathscr{R}_c$[a,b]

SYSTEMS	$\mathscr{R}_c$ 0.5	1.0	1.5	2.0	0.5[c]	1.5[c]
Swan (1, 0) / Swan (0, 0)	2.55 (−1) 2.08 (−1)	2.31 (−1) 1.67 (−1)	2.10 (−1) 1.46 (−1)	1.93 (−1) 1.34 (−1)	... ...	... ...
Phillips (0, 0) / Swan (0, 0)	8.52 (−2) 1.36 (−1)	1.14 (−1) 1.65 (−1)	1.30 (−1) 1.94 (−1)	1.41 (−1) 2.21 (−1)	... ...	... ...
Phillips (2, 0) / Swan (0, 0)	4.54 (−2) 6.79 (−2)	5.87 (−2) 7.99 (−2)	6.52 (−2) 9.24 (−2)	6.94 (−2) 1.05 (−1)	... ...	... ...
Phillips (0, 0) / Ballik-Ramsay (0, 0)	1.70 2.69	2.21 3.20	2.48 3.72	2.66 4.22	2.00 2.83	2.87 3.70
Ballik-Ramsay (0, 0) / Swan (0, 0)	5.00 (−2) 5.05 (−2)	5.16 (−2) 5.15 (−2)	5.25 (−2) 5.21 (−2)	5.30 (−2) 5.24 (−2)	... ...	... ...
$a\,^3\Pi_u$–$X\,^1\Sigma_g^+$ (0, 0) / Swan (0, 0)	5.86 (−6) 7.26 (−5)	2.63 (−5) 3.53 (−4)	6.49 (−5) 8.71 (−4)	1.24 (−4) 1.62 (−3)	... ...	... ...

[a] $\mathscr{R}_c$ is in AU.
[b] The upper and lower entry correspond to $|D_{a-X}|^2 = 10^{-5}$ and 10^{-4} a.u., respectively.
[c] Krishna Swamy and O'Dell 1987.

obtained from a least-squares fit to the values ln $[n(J'')/(2J''+1)]$ as a function of rotational energy $E(J'')$. From the excitation diagrams presented in Figure 2 it becomes clear that in some cases, most noticeably for the $d\,^3\Pi_g$ F_1 states, the population distribution among the rotational levels deviates from a thermal distribution at low J so that a single temperature fails to describe the populations of all levels properly. This problem is most severe for high values of the intercombination transition moment, $|D_{a-X}|^2 \geq 10^{-5}$ a.u. In many cases, however, a fairly good characterization of the population distribution is achieved by this approach. The linear correlation coefficients k for the least-squares fits vary between 0.95 and 1.0 for the values tabulated, except for the temperatures of levels in F_1, in which case k may be as low as 0.75–0.85. If, however, the least-squares fit is restricted to rotational levels $J = 20$–60, k increases to values around 0.95 and the characteristic rotational temperatures decrease significantly, as could be expected from the excitation diagrams presented in Figure 2. The vibrational temperature can be determined in two ways. Since the rotational structure is resolved, the most straightforward method would be to evaluate the mean excitation temperature determining the population density of a given rotational level in the various vibrational states. On the other hand, in the older literature the vibrational temperature is understood in terms of the population distribution among vibrational states, treating the population densities of the individual rotational levels as being collapsed into one vibrational level. Small deviations between the values obtained with the two methods are expected because the latter implies the assignment of the same excitation energy to all rotational levels. In the following tables, both values for the vibrational temperatures are presented. The vibrational excitation itself was found to follow very closely a thermal excitation at the temperatures tabulated in Table 5, with linear correlation coefficients generally close to one. This is in contrast with the results of Krishna Swamy and O'Dell (1977) and A'Hearn (1978, 1981, as cited by Lambert and Danks 1983), who found a decreasing excitation temperature with increasing v'.

In Table 5 the rotational temperatures in $v' = 0$ in the $A\,^1\Pi_u$ state and the three electronic substates of the $d\,^3\Pi_g$ state are given, as well as the vibrational temperatures for $J = 30$, and the mean vibrational temperatures. The rotational temperature in the $A\,^1\Pi_u$, $v' = 2$ level is also presented. Rotational temperatures are listed both for a fit to all J levels and for levels $J > 20$ only. The values for the $a\,^3\Pi_u$–$X\,^1\Sigma_g^+$ intercombination transition range from 10^{-8} to 10^{-3} a.u., and $|D_{c-X}|^2 = 0$. Both the vibrational and rotational temperatures decrease with increasing $|D_{a-X}|^2$, but the vibrational ladder is cooled more efficiently than the rotational one, in the sense that the vibrational temperature decreases more rapidly with increasing $|D_{a-X}|^2$. Very high values of the order of 10^{-4} a.u. for the $a\,^3\Pi_u$–$X\,^1\Sigma_g^+$ intercombination transition moment are required in order to cool the vibrational ladder in the $d\,^3\Pi_g$ state to the temperatures around 3000 K suggested by the observations of Lambert and Danks (1983). The rotational temperature, on the other hand, stays high, and even for $|D_{a-X}|^2 > 10^{-3}$ it is higher than 3000 K in the $d\,^3\Pi_g$ state. At low values of $|D_{a-X}|^2 < 10^{-5}$, the cooling of the vibrational ladder in the $d\,^3\Pi_g$ state is due to the inclusion of the $b\,^3\Sigma_g^-$–$a\,^3\Pi_u$ transitions. The value around 5000 K for vibrational levels in the $d\,^3\Pi_g$ state is in harmony with the results obtained by A'Hearn (1981, as cited in Lambert and Danks 1983).

ii) *Effect of the* $c\,^3\Sigma_u^+$–$X\,^1\Sigma_g^+$ *Transition*

The inclusion of the $c\,^3\Sigma_u^+$–$X\,^1\Sigma_g^+$ intercombination transitions affects both the flux ratios and the rotational temperatures, as Tables 6 and 7 demonstrate. Extreme values for $|D_{c-X}|^2$ in these tables illustrate the maximum possible effects of the $c\,^3\Sigma_u^+$–$X\,^1\Sigma_g^+$ transition. As indicated in Table 2, values of the order of $|D_{c-X}|^2 \approx 10^{-6}$–$10^{-5}$ a.u. are probably most realistic. The two values tabulated correspond to employed ratios A^{d-c}/A^{d-a} of 0.1 and 0.01 for the upper and lower value, respectively, and are meant to demonstrate the effects introduced by the strength of the $d\,^3\Pi_g$–$c\,^3\Sigma_u^+$ transition.

For a ratio of $A^{d-c}/A^{d-a} = 0.1$, it appears that the Swan (1, 0)/(0, 0) flux ratio is insensitive to $|D_{c-X}|^2$ for small $|D_{a-X}|^2 \approx$

TABLE 5

VIBRATIONAL AND ROTATIONAL TEMPERATURES AS FUNCTIONS OF THE $a\,^3\Pi_u$–$X\,^1\Sigma_g^+$ INTERCOMBINATION TRANSITION MOMENT[a,b]

	$\lvert D_{a-X}\rvert^2$						
STATE	10^{-8}	10^{-7}	10^{-6}	10^{-5}	10^{-4}	10^{-3}	c
Rotational temperature:							
$A\,^1\Pi_u$, $v=0$	4860	3790	3790	3390	3200	2760	3780
	4900	3740	3640	3510	3400	3070	4270
$A\,^1\Pi_u$, $v=2$	4270	3410	3410	3060	2890	2520	2930
	4300	3330	3330	3220	3140	2870	3340
$d\,^3\Pi_g$, F_1, $v=0$	4780	4980	5670	6560	5770	4580	8100
	4790	4990	5520	5850	4730	3870	5130
$d\,^3\Pi_g$, F_2, $v=0$	5830	5790	5510	4950	3960	3210	4680
	5510	5490	5520	5050	4060	3230	4920
$d\,^3\Pi_g$, F_3, $v=0$	6130	6040	5510	4610	3650	3240	4880
	5750	5790	5500	4910	3930	3420	4360
Vibrational temperature:							
$A\,^1\Pi_u$, $J=30$	4350	4330	4330	3930	3230	2870	4150
$d\,^3\Pi_g$, F_1, $J=31$	5180	5170	5090	4400	2850	1830	4840
$d\,^3\Pi_g$, F_2, $J=30$	5160	5140	4970	3930	2420	1620	4660
$d\,^3\Pi_g$, F_3, $J=29$	5050	5050	4950	4250	2780	1820	4860
$A\,^1\Pi_u$ mean	4180	4200	4200	3830	3280	3010	4130
$d\,^3\Pi_g$ mean	5190	5180	5070	4300	2930	2000	4850

[a] $\lvert D_{a-X}\rvert^2$ is in atomic units. The calculations are for $\mathcal{R}_c = 1.0$ AU and $v_c = -26.67$ km s^{-1}.

[b] See text for definition of the rotational and vibrational temperatures. The upper and lower entry tabulated for the rotational temperatures correspond to least-squares fits to rotational levels 3–60 and 20–60, respectively, as explained in the text.

[c] Obtained using the theoretical estimates for the $\lvert D_{a-X}\rvert^2$ transition moment (see § IIc and Table 2).

10^{-7} a.u., in which case it is almost equal to the value obtained without the $c\,^3\Sigma_u^+$–$X\,^1\Sigma_g^+$ transitions. For higher values of $\lvert D_{a-X}\rvert^2$, a weak dependence on $\lvert D_{c-X}\rvert^2$ develops. The main effect of the $c\,^3\Sigma_u^+$–$X\,^1\Sigma_g^+$ transition is manifested in a strong increase of the flux emitted in the singlet bands with respect to that in the triplet bands as $\lvert D_{c-X}\rvert^2$ increases. For low values of $\lvert D_{a-X}\rvert^2$ and $\lvert D_{c-X}\rvert^2 \neq 0$, almost the entire population density resides in the $X\,^1\Sigma_g^+$ state. This is by no means surprising since the $c\,^3\Sigma_u^+$–$X\,^1\Sigma_g^+$ intercombination transitions act in one way only; i.e., they transfer population density from the triplet to the singlet states, but not vice versa. At higher values of $\lvert D_{a-X}\rvert^2$, the $a\,^3\Pi_u$–$X\,^1\Sigma_g^+$ transition partly reshuffles the singlet population to the triplets via the $X\,^1\Sigma_g^+$–$a\,^3\Pi_u$ transition, resulting in an increase of the flux emitted in the triplet transitions with respect to the singlets. Note that the flux emitted in the $a\,^3\Pi_u$–$X\,^1\Sigma_g^+$ intercombination transition also

TABLE 6

FLUX RATIOS AS FUNCTIONS OF THE $c\,^3\Sigma_u^+$–$X\,^1\Sigma_g^+$ INTERCOMBINATION TRANSITION MOMENT[a,b]

	$\lvert D_{c-X}\rvert^2$					
	$\lvert D_{a-X}\rvert^2 = 10^{-7}$			$\lvert D_{a-X}\rvert^2 = 10^{-5}$		
SYSTEM	10^{-6}	10^{-4}	10^{-2}	10^{-6}	10^{-4}	10^{-2}
Swan (1, 0) / Swan (0, 0)	2.71 (−1)	2.72 (−1)	2.73 (−1)	2.48 (−1)	2.36 (−1)	2.35 (−1)
	2.60 (−1)	2.61 (−1)	2.61 (−1)	2.32 (−1)	2.32 (−1)	2.32 (−1)
Phillips (0, 0) / Swan (0, 0)	1.07	8.32	8.97	1.57 (−1)	5.54 (−1)	5.87 (−1)
	6.56 (−1)	8.95 (−1)	8.98 (−1)	1.33 (−1)	1.43 (−1)	1.43 (−1)
Phillips (2, 0) / Swan (0, 0)	5.53 (−1)	4.62	4.89	8.25 (−2)	2.92 (−1)	3.10 (−1)
	3.68 (−1)	5.02 (−1)	5.04 (−1)	6.97 (−2)	7.50 (−2)	7.51 (−2)
Phillips (0, 0) / Ballik-Ramsay (0, 0)	19.5	136.	145.	2.88	9.37	9.85
	12.1	16.4	16.4	2.50	2.67	2.67
Ballik–Ramsay (0, 0) / Swan (0, 0)	5.50 (−2)	6.12 (−2)	6.18 (−2)	5.46 (−2)	5.91 (−2)	5.96 (−2)
	5.45 (−2)	5.47 (−2)	5.47 (−2)	5.33 (−2)	5.35 (−2)	5.35 (−2)
$a\,^3\Pi_u$–$X\,^1\Sigma_g^+$ / Swan (0, 0)	2.25 (−6)	1.73 (−5)	3.41 (−5)	1.79 (−5)	3.10 (−5)	3.19 (−5)
	4.12 (−7)	4.25 (−7)	4.25 (−7)	4.05 (−5)	4.05 (−5)	4.05 (−5)

[a] All transition moments are in atomic units.

[b] Obtained using the theoretical oscillator strengths of van Dishoeck 1983 for the Phillips system, and a heliocentric distance and velocity of the absorbers of $\mathcal{R}_c = 1.0$ AU and $v_c = -26.67$ km s^{-1}. The upper and lower value presented for each entry correspond to values of 0.1 and 0.01, respectively, for the ratio A^{d-c}/A^{d-a}.

TABLE 7

VIBRATIONAL AND ROTATIONAL TEMPERATURES AS FUNCTIONS OF THE $c\,^3\Sigma_u^+ - X\,^1\Sigma_g^+$ INTERCOMBINATION TRANSITION MOMENT[a,b]

	$\lvert D_{c-X}\rvert^2$					
	$\lvert D_{a-X}\rvert^2 = 10^{-7}$			$\lvert D_{a-X}\rvert^2 = 10^{-5}$		
STATE	10^{-6}	10^{-4}	10^{-2}	10^{-6}	10^{-4}	10^{-2}
Rotational temperature:						
$A\,^1\Pi_u$, $v = 0$	5100	5100	5090	2800	2270	2240
	5260	5470	5470	2950	2910	2910
$A\,^1\Pi_u$, $v = 2$	4320	4330	4340	2520	2070	2050
	3810	3920	3920	2310	2290	2290
$d\,^3\Pi_g$, F_1, $v = 0$	6470	6390	6390	4290	2790	2730
	5400	5520	5520	4340	4150	4150
$d\,^3\Pi_g$, F_2, $v = 0$	5060	5010	5010	3700	2520	2460
	4700	4700	4700	3810	3650	3650
$d\,^3\Pi_g$, F_3, $v = 0$	5270	5230	5220	3510	2560	2510
	4850	4870	4870	3470	3380	3380
Vibrational temperature:						
$A\,^1\Pi_u$, $J = 30$	4340	4340	4100	4040	4020	4020
	4250	4250	4250	3850	3850	3850
$d\,^3\Pi_g$, F_1, $J = 31$	5210	5230	5240	4810	4550	4530
	5100	5110	5110	4350	4340	4340
$d\,^3\Pi_g$, F_2, $J = 30$	4970	5130	5140	4350	4130	4120
	5170	5180	5180	4000	3980	3980
$d\,^3\Pi_g$, F_3, $J = 29$	5120	5110	5110	4640	4410	4390
	5180	5180	5180	4320	4310	4310
$A\,^1\Pi_u$ mean	4250	4250	4060	3990	4000	4000
	4200	4200	4200	3850	3850	3850
$d\,^3\Pi_g$ mean	5160	5160	5160	4670	4350	4330
	5220	5220	5220	4310	4290	4290

[a] All transition moments are in atomic units.

[b] See text for definition of the rotational and vibrational temperatures. Only rotational levels $J = 20$–60 were used in the determination of the rotational temperature. The upper and lower value presented for each entry correspond to values of 0.1 and 0.01, respectively, for the ratio A^{d-c}/A^{d-a}.

increases with increasing strength of the $c\,^3\Sigma_u^+ - X\,^1\Sigma_g^+$ intercombination transition. This effect corresponds to the decay of $d\,^3\Pi_g$ density via the $d\,^3\Pi_g - c\,^3\Sigma_u^+ - X\,^1\Sigma_g^+$ cascade. In the case of a weak $d\,^3\Pi_g - c\,^3\Sigma_u^+$ transition, the triplet-singlet conversion via the $c\,^3\Sigma_u^+$ state becomes much less pronounced. A decrease by a factor of 10 in the strength of $d\,^3\Pi_g - c\,^3\Sigma_u^+$ transitions results in a decrease of the relative population density in the singlet states with respect to the triplet states by a similar factor, as long as the $c\,^3\Sigma_u^+ - X\,^1\Sigma_g^+$ transition is more efficient in depopulating the $c\,^3\Sigma_u^+$ levels than absorptions to the $d\,^3\Pi_g$ state. This appears to be the case for values of $\lvert D_{c-X}\rvert^2$ higher than $\sim 10^{-5}$ a.u. On the other hand, for small values of $\lvert D_{c-X}\rvert^2$ the intercombination transitions become negligible and the triplet-singlet conversion through the $c\,^3\Sigma_u^+$ state reaches an equilibrium value which depends only on the strength of the $c\,^3\Sigma_u^+ - X\,^1\Sigma_g^+$ intercombination transition. This is a consequence of the population density in $c\,^3\Sigma_u^+$ reaching its maximal value, independent of the $d\,^3\Pi_g - c\,^3\Sigma_u^+$ transition moment as discussed in § IIc.

The inclusion of the $c\,^3\Sigma_u^+ - X\,^1\Sigma_g^+$ intercombination transitions has only a small influence on the vibrational temperature. This result is in agreement with the findings by Krishna Swamy and O'Dell (1987) and is illustrated in Table 7. The two values tabulated correspond to $A^{d-c}/A^{d-a} = 0.1$ and 0.01 for the upper and lower entry, respectively. The vibrational temperatures presented for the various states change by less than 10% as $\lvert D_{c-X}\rvert^2$ increases from 10^{-6} to 10^{-2} and are almost equal to the values obtained without the $c\,^3\Sigma_u^+ - X\,^1\Sigma_g^+$ transition. There is only a very weak dependence of the vibrational temperature on the strength of the $d\,^3\Pi_g - c\,^3\Sigma_u^+$ transition. On the other hand, the inclusion of the $c\,^3\Sigma_u^+ - X\,^1\Sigma_g^+$ system strongly affects the rotational temperature. In general, the rotational temperature decreases rapidly with increasing $\lvert D_{c-X}\rvert^2$, if the $d\,^3\Pi_g - c\,^3\Sigma_u^+$ and $a\,^3\Pi_u - X\,^1\Sigma_g^+$ transitions are sufficiently strong. Note that low rotational temperatures in the $d\,^3\Pi_g$ states, $T_{\rm rot} \simeq 3500$ K are obtained already for $\lvert D_{a-X}\rvert^2 \approx \lvert D_{c-X}\rvert^2 \approx 10^{-6}$–$10^{-5}$ a.u. The strong dependence of the rotational temperature on the value of $\lvert D_{c-X}\rvert^2$ vanishes if the strength of the $d\,^3\Pi_g - c\,^3\Sigma_u^+$ transition is diminished to $A^{d-c}/A^{d-a} = 0.01$, and even for unrealistically high values of the $c\,^3\Sigma_u^+ - X\,^1\Sigma_g^+$ intercombination transition moment it stays higher than 3000 K.

Summarizing the results for the excitation temperatures, it can be concluded that the vibrational temperature is almost exclusively determined by the strength of the $a\,^3\Pi_u - X\,^1\Sigma_g^+$ transition, whereas the rotational temperature depends on the strength of both intercombination transitions. As far as the emission in the various bands is concerned, the intensities of the singlet bands increase strongly with increasing strength of the $c\,^3\Sigma_u^+ - X\,^1\Sigma_g^+$ transition if the $d\,^3\Pi_g - c\,^3\Sigma_u^+$ transition is sufficiently rapid, whereas the combined effects of the $a\,^3\Pi_u - X\,^1\Sigma_g^+$ and the $X\,^1\Sigma_g^+ - a\,^3\Pi_u$ transitions balance the population distribution among singlet and triplet states. The change in heliocentric distance of the absorbers has noticeable effects on the vibrational and rotational temperatures and the singlet to triplet flux ratios.

TABLE 8

VIBRATIONAL AND ROTATIONAL TEMPERATURES AS FUNCTIONS OF HELIOCENTRIC DISTANCE $\mathscr{R}_c$[a,b]

STATE	$\mathscr{R}_c$ 0.5	1.0	1.5	2.0	1.1[c]	1.1[d]
Rotational temperature:						
$A\,^1\Pi_u, v = 0$	3520	2710	2290	2560	3810	2630
	3230	2480	2110	2060		
$A\,^1\Pi_u, v = 2$	2770	2200	1880	1700	3060	2140
	2570	2020	1740	1700		
$d\,^3\Pi_g, F_1, v = 0$	4660	3490	2870	2530	4760	3340
	4320	3190	2620	2530		
$d\,^3\Pi_g, F_2, v = 0$	3990	3070	2580	2310	4230	2830
	3730	2830	2380	2310		
$d\,^3\Pi_g, F_3, v = 0$	4040	3090	2590	2320	4160	3420
	3760	2840	2390	2320		
Vibrational temperature:						
$A\,^1\Pi_u, J = 30$	4170	4000	3880	3770	4170	4010
	4100	3910	3760	3770		
$d\,^3\Pi_g, F_1, J = 31$	5160	4620	4170	3830	4690	4590
	5130	4570	4120	3830		
$d\,^3\Pi_g, F_2, J = 30$	5120	4450	3920	3530	4540	4610
	5060	4370	3850	3530		
$d\,^3\Pi_g, F_3, J = 29$	5220	4670	4200	3840	4700	4770
	5190	4620	4150	3840		
$A\,^1\Pi_u$ mean	4150	4020	3910	3810	4160	4030
	4090	3930	3800	3810		
$d\,^3\Pi_g$ mean	5300	4640	4120	3730	4730	4730
	5260	4580	4060	3730		

[a] $\mathscr{R}_c$ is in AU.

[b] All calculations use $|D_{a-X}|^2 = |D_{c-X}|^2 = 3.5 \times 10^{-6}$ a.u. and $A^{d-c}/A^{d-a} = 0.1$, unless otherwise indicated. The upper and lower entries employ the theoretical and the experimental lifetimes for the Phillips system, respectively. The rotational levels $J = 20$–60 were used in the determination of the rotational temperature.

[c] Obtained using the theoretical estimates for the $|D_{a-X}|^2$ and $|D_{c-X}|^2$ transition moments (see § IIc and Table 2).

[d] Obtained using the theoretical transition probabilities of Le Bourlot and Roueff 1986 for $J < 30$.

iii) *Synthetic Spectra*

Anticipating the results of the next section, we find that values of $|D_{a-X}|^2 \approx |D_{c-X}|^2 \approx 3.5 \times 10^{-6}$ a.u. fit best the observed spectra of the C_2 (0, 0) Swan band in comet Halley, if A^{d-c}/A^{d-a} is as large as 0.1. Although most subsequent results will be presented for this set of parameters, it should be noted that for $A^{d-c}/A^{d-a} = 0.02$–0.03, the value suggested by the quantum chemical calculations of Klotz (1987), an equally good fit is obtained with a similar value for $|D_{a-X}|^2$, but with $|D_{c-X}|^2$ increased to 2×10^{-5} a.u. In Tables 8 and 9, the vibrational and rotational temperatures and the various flux ratios are presented as functions of the heliocentric distance of the comet, adopting the former values for the intercombination transition moments and the $d\,^3\Pi_g$–$c\,^3\Sigma_u^+$ strength. The two values tabulated for each $\mathscr{R}_c$ correspond to the use of theoretical and experimental values for the lifetime of the Phillips system, respectively. In addition, the results obtained with the estimated values of both the $|D_{a-X}|^2$ and $|D_{c-X}|^2$ transition moments (see § IIc) are listed, together with a calculation in which the theoretical individual rotational transition probabilities of Le Bourlot and Roueff (1986) were adopted for the $a\,^3\Pi_u$–$X\,^1\Sigma_g^+$ transitions. In the latter case, the probabilities for rotational levels $J > 30$ and for all levels in the $c\,^3\Sigma_u^+$ state were calculated using $|D_{a-X}|^2 = |D_{c-X}|^2 = 3.5 \times 10^{-6}$ a.u. It appears that the vibrational temperatures in the $d\,^3\Pi_g$ electronic substates are not much affected if the theoretical estimates (see Table 2) are adopted, whereas the rotational temperatures are significantly higher. With the detailed theoretical values of Le Bourlot and Roueff (1986) both the vibrational and rotational temperatures are similar to those obtained with the constant transition moment. The only exceptions are the F_2 levels, which are cooled more efficiently with the detailed values because their transition probabilities are an order of magnitude larger than those for the F_1 and F_3 levels according to Le Bourlot and Roueff (1986).

The findings for the vibrational temperatures are also reflected, for example, in the Swan (1, 0)/(0, 0) flux ratios listed in Table 9. The largest sensitivity to the adopted intercombination transition moments is found for the Phillips/Swan flux ratios. This results from the fact that the theoretical calculations do not give equal probabilities for singlet-triplet transitions and for triplet-singlet transitions. The theoretical lieftimes of Le Bourlot and Roueff (1986) suggest that the singlet-triplet conversion is less efficient than the triplet-singlet conversion, so that with their limited set of values some increase in singlet-triplet population is noticed. For instance, the inverse radiative lifetimes of rotational levels in the (1, 0) band of the $a\,^3\Pi_u$–$X\,^1\Sigma_u^+$ transition are of the order of 10^{-3} s^{-1}, whereas the corresponding values for the (1, 0) band of the $X\,^1\Sigma_g^+$–$a\,^3\Pi_u$ transition are 5–10 times smaller.

Table 9 also confirms the expectations that the various band ratios within the triplet or singlet states are not sensitive to the adopted Phillips band oscillator strengths and that the $a\,^3\Pi_u$–$X\,^1\Sigma_g^+$ (0, 0) band strength shows only a weak dependence. The emitted fluxes in the Phillips bands decrease, of course, almost linearly with decreasing oscillator strength.

In Figures 3*a*–3*c*, synthetic emission profiles for a heliocentric distance of 1.1 a.u. and a heliocentric velocity of -26.67 km s^{-1} are presented. The solid line in each figure corresponds to the "reference" model with $|D_{a-X}|^2 = |D_{c-X}|^2 = 3.5 \times 10^{-6}$ a.u. and $A^{d-c}/A^{d-a} = 0.1$. It is compared with dotted profiles which correspond to (*a*) $|D_{a-X}|^2 = |D_{c-X}|^2 = 3.5 \times 10^{-6}$ a.u., but with an additional dilution of the solar radiation by a factor of 2.25, (*b*) to the use of the estimated values for both $|D_{a-X}|^2$ and $|D_{c-X}|^2$ according to Table 2, and (*c*) to the use of the detailed theoretical probabilities (Le Bourlot and Roueff 1986).

It is interesting to note that the difference between the synthetic profiles using the estimated values of the transition moment and those provided by Le Bourlot and Roueff (1986) is not very pronounced, although the estimated values of $|D_{a-X}|^2$ differ by factors of a few. The reason for this result is twofold. First, the $a\,^3\Pi_u$–$X\,^1\Sigma_g^+$ transition probabilities of Le Bourlot and Roueff (1986) were limited to $J' < 30$, yet the spectra presented in Figure 3 are dominated by high rotational lines around $J \approx 40$, for which $|D_{a-X}|^2 = 3.5 \times 10^{-6}$ a.u. has been adopted. Second, the similarity probably reveals the importance of a proper theoretical calculation of the rotational lifetimes due to the intercombination transitions. Much higher effective values for the rotational line probabilities are obtained as soon as the rotational dependences of the perturbing Hamiltonian are included, instead of only the vibrational structure. This consideration also shows that the estimated values for $|D_{a-X}|^2$ and $|D_{c-X}|^2$ listed in Table 2 are likely to be lower limits to the effective intercombination transition moments that determine the rotational transition probabilities.

TABLE 9

FLUX RATIOS AS FUNCTIONS OF HELIOCENTRIC DISTANCE $\mathscr{R}_c$[a,b]

SYSTEM	$\mathscr{R}_c$ 0.5	1.0	1.5	2.0	1.1[c]	1.1[d]
Swan (1, 0) / Swan (0, 0)	2.65 (−1) 2.64 (−1)	2.47 (−1) 2.44 (−1)	2.29 (−1) 2.24 (−1)	2.14 (−1) 2.14 (−1)	2.37 (−1)	2.50 (−1)
Phillips (0, 0) / Swan (0. 0)	3.15 (−1) 2.01 (−1)	3.62 (−1) 2.52 (−1)	3.56 (−1) 2.58 (−1)	3.40 (− 1) 1.70 (−1)	2.36 (−1)	4.18 (−1)
Phillips (2, 0) / Swan (0, 0)	1.76 (−1) 1.10 (−1)	1.97 (−1) 1.35 (−1)	1.91 (−1) 1.36 (−1)	1.81 (−1) 9.03 (−2)	1.32 (−1)	2.29 (−1)
Phillips (0, 0) / Ballik-Ramsay (0, 0)	5.98 3.82	6.37 4.44	5.96 4.34	5.55 2.77	4.39	7.30
Ballik-Ramsay (0, 0) / Swan (0, 0)	5.27 (−2) 5.26 (−2)	5.68 (−2) 5.68 (−2)	5.97 (−2) 5.95 (−2)	6.13 (−2) 6.13 (−2)	5.38 (−2)	5.75 (−2)
$a\,^3\Pi_u$–$X\,^1\Sigma_g^+$(0, 0) / Swan (0, 0)	3.71 (−6) 3.77 (−6)	1.84 (−5) 1.92 (−5)	4.85 (−5) 5.02 (−5)	9.44 (−5) 6.83 (−5)	1.59 (−6)	1.49 (−5)

[a] $\mathscr{R}_c$ is in AU.

[b] All calculations use $|D_{a-X}|^2 = |D_{c-X}|^2 = 3.5 \times 10^{-6}$ a.u. and $A^{d-c}/A^{d-a} = 0.1$, unless otherwise indicated. The upper and lower entries employ the theoretical and the experimental lifetimes for the Phillips system, respectively. The rotational levels $J = 20$–60 were used in the determination of the rotational temperature.

[c] Obtained using the theoretical estimates for the $|D_{a-X}|^2$ and $|D_{c-X}|^2$ transition moments (see § IIc and Table 2).

[d] Obtained using the theoretical transition probabilities of Le Bourlot and Roueff 1986 for $J < 30$.

IV. COMPARISON WITH OBSERVATIONS

a) C_2 (0, 0) *Swan Band Observations*

The (0, 0) Swan band in comet Halley was observed on 1985 December 26–27 with the echelle spectrograph at the Multiple Mirror Telescope at Mount Hopkins, Arizona. Spectra were obtained both at the nucleus position, and at a 2″W, 2″S sunward offset position. The slit width was set to 100 μm, corresponding to 1.″2 projected on the sky, yielding a resolution $\lambda/\Delta\lambda \approx 24{,}000$ (i.e., $\Delta\lambda = 0.21$ Å at $\lambda = 5160$ Å). The total integration times were 1 hr for the nucleus spectra and 1.5 hr for the coma spectra. Spectra were obtained with the same instrumental setup of reflected sunlight from the twilight sky at the beginning of the evening and of the moonlit sky after the cometary observations. These spectra were properly scaled and subtracted from the cometary spectra in order to remove the contribution of scattered sunlight from the cometary emission. The accurate removal of the strong Mg I lines of the Fraunhofer spectrum just longward of the Swan (0, 0) band head shows that this procedure was carried out satisfactorily. From the flux longward of the (0, 0) band head, the contribution of scattered sunlight was found to be 17% of the peak intensity of C_2 emission in the nucleus spectrum, and 6% of the peak in the coma spectrum. All spectra have been corrected for the appropriate Doppler shifts at the times of observation: the final spectra reproduced in Figures 4*a* and 4*b* have a linear wavelength scale at rest in the heliocentric frame. The normalizations of the flux scales correspond to 2150 and 2490 counts per pixel for the nucleus and coma spectra, respectively.

The nucleus and coma spectra of the C_2 (0, 0) Swan band region are heavily contaminated by NH_2 emission lines. In both Figures 4*a* and 4*b*, the positions of the NH_2 $\tilde{A}\,^2A_1$–$\tilde{X}\,^2B_1$ (0, 12, 0) lines are indicated by small vertical bars. The identification is based on wavenumbers tabulated by Dressler and Ramsay (1959). A detailed analysis of the amount of NH_2 contamination in low-resolution C_2 spectra of comet Halley as a function of distance from the nucleus has been performed by Di Santi and Fink (1987). High-resolution spectra of comet Halley were also obtained with the MMT echelle spectrograph on 1985 October 27–28 and 1986 May 4–5 when the comet was at $\mathscr{R}_c = 2$ AU preperihelion and $\mathscr{R}_c = 2$ AU postperihelion, respectively. Furthermore, emission in the (2, 0) band was recorded in December. Although the strongest rotational line features of the respective bands are evident, the signal/noise ratio in these spectra is rather low, and they will not be discussed further with reference to the detailed, high-resolution analysis.

Synthetic profiles were calculated for values of $\mathscr{R}_c = 1.1$ AU and $v_c = -26.7$ km s^{-1}, corresponding to the heliocentric distance and the heliocentric velocity of comet Halley on December 26. The geocentric distance at the time of the observations was 1 AU. The theoretical spectra are indicated by individual dots in Figures 4*a* and 4*b*. The theoretical spectrum in Figure 4*b*, obtained with $|D_{a-X}|^2 = |D_{c-X}|^2 = 3.5 \times 10^{-6}$ a.u. and with $A^{d-c}/A^{d-a} = 0.1$, agrees very well with the coma spectrum of comet Halley. As mentioned in § III, a similarly good fit is obtained for $A^{d-c}/A^{d-a} \approx 0.03$ when $|D_{c-X}|^2 = 2 \times 10^{-5}$ a.u. Although the fit is not unique, the fact that a good fit can be obtained with reasonable parameters suggests that indeed the excitation of the rotational levels can be understood in terms of resonance fluorescence, as appears to be the case for the vibrational levels. The population density among the rotational levels is characterized by a mean temperature around 3000 K. From the present spectra it is not possible to determine the vibrational temperature, since no simultaneous well-calibrated observations of rotational lines in other bands were obtained. However, with the adopted values of the intercombination transition moments, vibrational temperatures of 4300–4600 K in the $d\,^3\Pi_g$ states are predicted. A confirmation of this prediction is discussed below. For comparison, Lambert and Danks (1983) found a similar rotational temperature $T_{rot} \approx 3500$ K for comet West at $\mathscr{R}_c = 0.78$ AU, but inferred a lower vibrational temperature $T_{vib} \approx (3500 \pm 400)$ K than is suggested for comet Halley at $\mathscr{R}_c = 1.1$ AU.

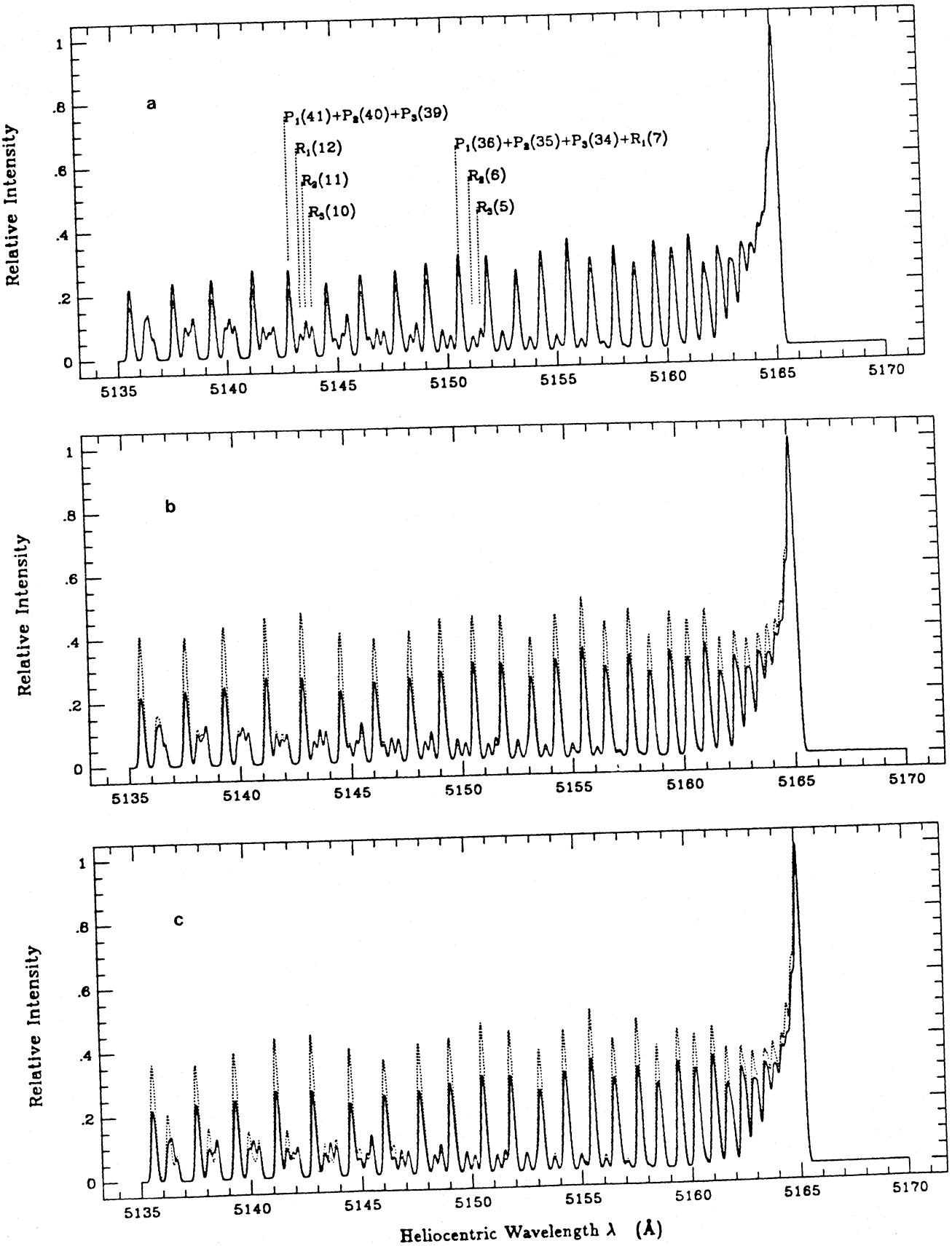

FIG. 3.—Synthetic profile for the C_2 (0, 0) Swan band at 0.2 Å resolution, obtained with $|D_{a-X}|^2 = |D_{c-X}|^2 = 3.5 \times 10^{-6}$ a.u., $A^{d-c}/A^{d-a} = 0.1$, $\mathscr{R}_c = 1.1$ AU, and $v_c = -26.67$ km s^{-1} (*solid line*) is compared to (*a*) a synthetic spectrum obtained with an additional dilution of the solar radiation field of 2.25; (*b*) a spectrum obtained with the estimated values of the intercombination transition moments as presented in Table 2; and (*c*) a synthetic model calculated with the theoretical values for the transition probabilities of rotational levels in the $a\,^3\Pi_u$–$X\,^1\Sigma_g^+$ transition (Le Bourlot and Roueff 1986). In (*a*), a number of rotational lines and line blends are indicated explicitly.

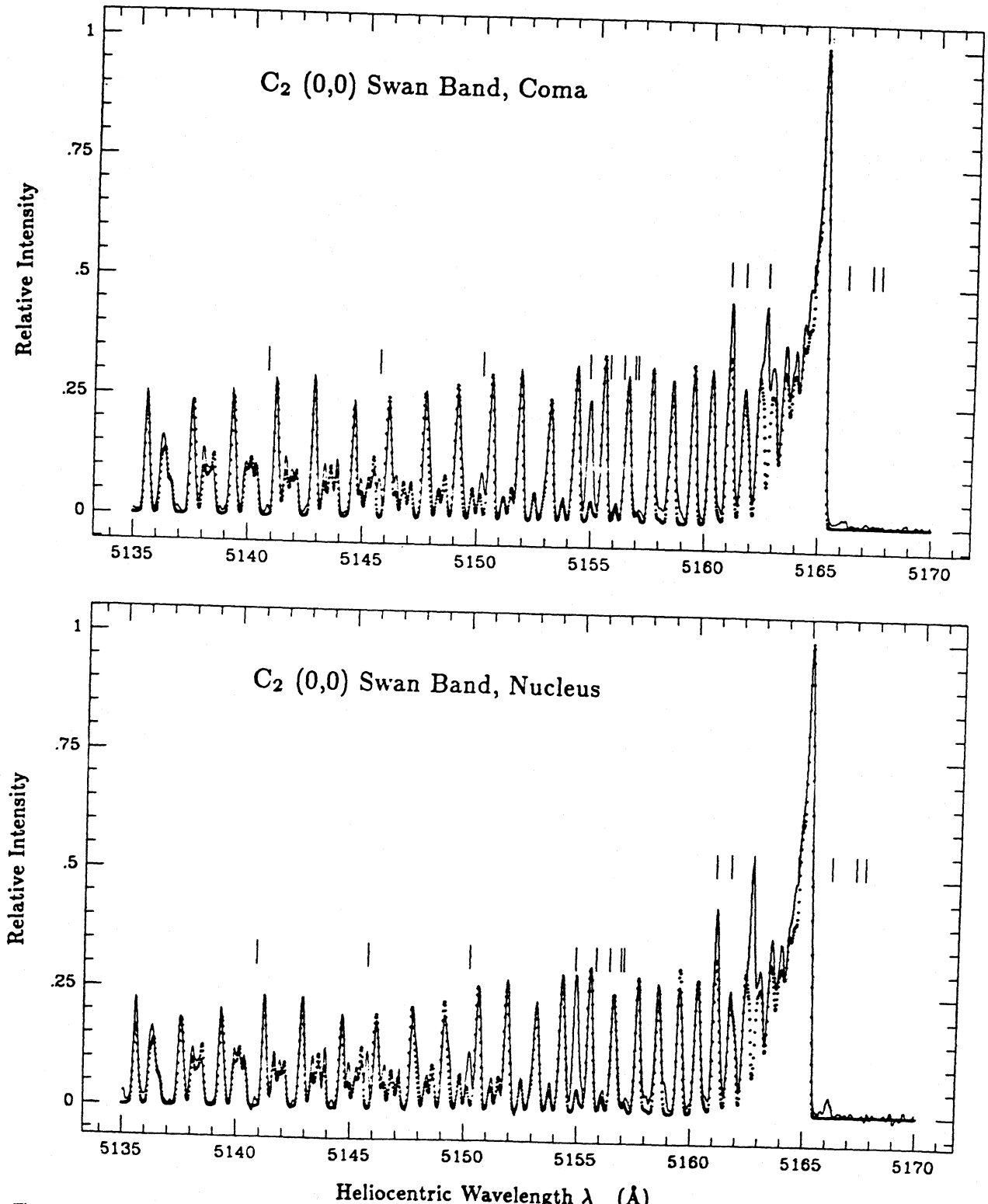

FIG. 4.—The observed coma (*a*) and nucleus spectrum (*b*) of the (0, 0) Swan band at a resolution of 0.2 Å obtained at the MMT (*solid line*). Theoretical spectra, obtained with $|D_{a-X}|^2 = |D_{c-X}|^2 = 3.5 \times 10^{-6}$ a.u. (see Fig. 3), are presented by the dotted lines. In (*b*), an additional dilution factor of 2.25 is employed. Small vertical bars indicate the positions of NH_2 lines.

If either the theoretical estimates for the intercombination moments (see § IIc, Table 2) or the $a\,^3\Pi_u$–$X\,^1\Sigma_g^+$ data provided by Le Bourlot and Roueff (1986) are employed, differences between the synthetic spectra and the observations emerge. The magnitudes of these differences have already been illustrated in Figures 3*a*–3*c*. The discrepancies are not very large, but are measurable. Definite conclusions must await further calculations similar to those presented by Le Bourlot and Roueff (1986), but extended to higher rotational levels and to the $c\,^3\Sigma_u^+$–$X\,^1\Sigma_g^+$ transition.

b) Coma versus Nucleus Spectra

If the C_2 spectra of comet Halley at the nucleus and coma positions are compared carefully, a difference in rotational line intensities becomes apparent. The higher rotational levels $J \gtrsim 24$ appear to be more highly populated at the coma position than at the nucleus position. This is readily recognized, for example, by comparison of the intensities of the lines with the identification bars for the NH_2 lines, which are plotted at the same height in both spectra in Figure 4. The C_2 rotational temperature at the nucleus position is ~ 500 K lower than that at the coma position.

The differences between the nucleus and coma spectra are very interesting and may reveal some insight into the physical processes occurring in the inner coma. If, indeed, the same generation of C_2 molecules is observed in both cases, the observed differences may be due to different excitation conditions for the C_2 molecule at the two positions. In that case, there are three major processes in the inner coma that may cause the observed differences, namely (i) deviations from statistical equilibrium; (ii) redistribution of population density by collisions; and (iii) a shielding of the solar radiation field by dust particles. For the following discussions, the physical parameters presented by Huebner (1986) for comae of bright comets are used. Although C_2 is a secondary or tertiary molecule of uncertain parentage, its abundance in the inner coma is high and stays constant until the distance from the cometary nucleus reaches a few thousand kilometers (Cochran 1985). At the time of the observation, the geocentric distance was 1.06 AU; therefore, the 2″W and 2″S offset of the spectrograph slit corresponded to 2174 km. With an outflow velocity of 1 km s^{-1}, the time necessary to cover this distance is much smaller than the mean lifetime of C_2 due to photodissociation, which is at least 10^5 s (A'Hearn, Thurber, and Mills 1977; Cochran 1985). The observed differences between the two spectra can therefore be interpreted as differences in the C_2 excitation. If the total density of molecules near the cometary nucleus is taken to be of order 10^{13} cm^{-3}, the collision rate is ~ 200 s^{-1} per C_2 molecule, assuming that the collisional cross section for C_2 is 2×10^{-16} cm^2, about half its geometrical cross section. The collision rate decreases rapidly with increasing time as the molecules stream outward, owing to the r^{-2} variation of total density. From Figure 1 presented by Huebner (1986), it appears that at a distance of only 30 km the density has decreased by a factor of 1000, which is large enough to bring the collision rate below the rate of excitation in the solar radiation field, ~ 0.3 s^{-1} in the Swan lines (Lambert and Danks 1983). A C_2 molecule produced in the immediate neighborhood of the nucleus will spend ~ 30 s in the collision-dominated inner coma. Within this time, it will undergo about 1000 collisions. The formation of C_2 most probably results in molecules with a very nonthermal population distribution among the vibrational and rotational levels, but the large number of collisions would wipe out the original population distribution and would tend to establish a value close to the kinetic temperature in the inner coma, which is ~ 150 K. As the molecules move farther out, they are exposed only to the intense solar radiation field, thereby establishing the excitation temperatures of the rovibrational levels as discussed in the previous section. The width of the spectrograph slit corresponds to 923 km at the distance of the comet, and molecules produced near the nucleus will undergo a few hundred upward transitions before they leave the region mapped by the observation with the slit centered on the cometary nucleus. Before the molecules travel into the region detected by the spectrograph slit set 2″ off the nucleus, corresponding to a distance of 2000 km, they will undergo some hundred additional transitions.

Even with allowance for the uncertainties in the intersystem transition moments, the lifetime of $a\,^3\Pi_u$ ($v = 0$) levels against transitions to $X\,^1\Sigma_g^+$ ($v = 0$), $\tau \approx 10^3$–10^5 s, is longer than or comparable to the flow time scale. Thus it may be that full statistical equilibrium including all processes that govern the rotational and vibrational temperatures in the lowest states is not achieved within a few thousand kilometers of the nucleus. For a higher v in the $a\,^3\Pi_u$ state, however, the lifetime against intercombination transitions is much shorter, and statistical equilibrium for higher v levels is probably reached. It is thus likely that the dominant process that governs the $a\,^3\Pi_u$ $v = 0$ population is not the a–X (0, 0) transition, but rather fluorescent excitation followed by intercombination transitions involving higher v, so that the $v = 0$ population is expected to approach statistical equilibrium.

The observed rotational temperature for $J > 7$—the J value for which individual R_i lines become partially resolved—is far from 150 K, thereby ruling out collisions as a major effect in determining the population distribution of C_2 detected near the nucleus. From the facts that the collisions dominate only in the inner 10% of the observed region and that C_2 is not a primary molecule with maximum abundance in the close neighborhood of the nucleus, it is unlikely that collisions play even a small role in the excitation. The dominant effect causing the excitation difference near the nucleus may be the shielding of the solar radiation field by dust particles released from the nucleus. This is supported by a comparison of theoretical and observed spectra in which the effect of additional dust shielding is mimicked by a dilution factor that differs from the purely geometrical one. In Figure 4*b*, the nucleus spectrum is illustrated together with a theoretical profile computed with an additional dilution of the solar radiation field of a factor 2.25, but with the same $|D_{a-X}|^2 = |D_{c-X}|^2 = 3.5 \times 10^{-6}$ a.u. as determined from the coma spectra. The agreement is excellent. An attenuation by a factor of 2.25 corresponds to an opacity $\tau_V \approx 0.8$ in the visible.

After this manuscript was submitted for publication, we received a preprint by O'Dell *et al.* (1988) describing detailed low-resolution measurements of the dependence of the C_2 excitation on distance from the nucleus. They estimate that the visible optical depth of the coma was $\tau < 0.01$ at projected distances greater than 100 km during the period 1985 October to 1986 March, so that our suggestion of opacity effects may be untenable. O'Dell *et al.* suggest that the abnormal band-sequence flux ratios in the most inner part of the coma (<100 km) might be caused by a C_2 formation process with a higher vibrational (and possibly also rotational) temperature than the equilibrium value. They derive a value for the inter-

combination transition moment $|D_{a-X}|^2$ of 2×10^{-6} a.u., close to the value found in this work. Vanysek, Valníček, and Sudova (1988) have also presented measurements of the $\Delta v = +1/\Delta v = 0$ band sequence flux ratio into a projected distance of 200 km.

c) *Comparison with Other Observations*

For comet Halley, a number of additional measurements of C_2 spectra exist. Rotational emission lines in the Swan (1, 1) and (0, 0) bands were obtained by Wehinger *et al.* (1986) with the coudé echelle spectrograph and an intensified-CCD photon counting system at the 1.8 m Mount Stromlo telescope. The $1'' \times 21''$ spectrograph slit was centered on the nucleus and extended across a substantial region of the coma. The spectrum covers the 5125–5145 Å region and has a resolution of ~100,000. A synthetic profile, employing values of $|D_{a-X}|^2 = |D_{c-X}|^2 = 3.5 \times 10^6$ a.u. with $A^{d-c}/A^{d-a} = 0.1$, was calculated for a heliocentric distance of 1.28 AU and a heliocentric velocity of 26.7 km s^{-1}, corresponding to the comet's distance and velocity at the time of the observation. Note that with the higher resolution, the individual R_1, R_2, and R_3 lines are resolved. Figures 5*a*–5*c* illustrate the spectra in the $\Delta v = 1$, 0, and -1 band sequences up to $v' = 5$ at a resolution of 0.2 Å. A detailed comparison between the synthetic fit and the observations will be presented elsewhere (Wehinger *et al.* 1986, 1989), but the agreement is generally good. In particular, the relative intensities of rotational lines in the (1, 1) band with respect to lines in the (0, 0) band are satisfactorily reproduced. Since this ratio is directly related to the vibrational temperature, it is suggested that the parameter set of $|D_{a-X}|^2 = |D_{c-X}|^2 = 3.5 \times 10^{-6}$ a.u. describes both the rotational temperature and the vibrational temperature in the Swan bands properly. The close agreement between the observed and theoretical vibrational temperature is a strong support of the model presented here, since the adopted parameters were obtained from a fit of the (0, 0) Swan band with no information about the vibrational temperature.

High-resolution spectra of the (0, 0) Swan band have also been obtained by Arpigny *et al.* (1986) in 1986 March with the ESO coudé echelle spectrometer at the 1.4 m CAT telescope at La Silla when $\mathscr{R}_c = 0.85$ AU. A preliminary spectrum with a resolution around 100,000 was presented, but no further details about the excitation have yet been published. According to the present calculations, the rotational excitation temperature should have increased by a few hundred degrees at $\mathscr{R}_c = 0.84$ AU compared with $\mathscr{R}_c = 1.1$ AU.

High-resolution observations of the Phillips $A\,^1\Pi_u$–$X\,^1\Sigma_g^+$ (2, 0) band centered on the nucleus of comet Halley were made by Appenzeller and Münch (1987) with the 3.6 m telescope at La Silla in 1986 March. The spectra cover the 8100–9100 Å range and have a resolution of ~0.45 Å. The spectra in the 8600–8900 Å region are contaminated by telluric features of the (7, 3) band of OH, but most of the low rotational C_2 lines appear well separated from this airglow emission. Highly excited rotational lines, such as the $R(36)$ line, appear with strong intensity in the spectrum. Unfortunately, the measurement of other highly excited rotational lines is complicated by the additional appearance of telluric H_2O and cometary CN lines at $\lambda > 8900$ Å. From the intensities of the measured C_2 lines, population densities in the upper rotational levels were inferred, but the measurements reveal an appreciable scatter and a proper determination of a rotational temperature cannot be made. The present calculations clearly predict a low rotational temperature, $T_{rot} < 3000$ K (see Table 8), for the comet at $\mathscr{R}_c = 0.75$–0.76. Figures 5*d*–5*f* illustrate the theoretical spectra of the (2, 0) and (1, 0) Phillips bands at a resolution of 0.4 Å, together with emission in the (2, 0) band of the Ballik-Ramsay system. It appears that emission in the Ballik-Ramsay system is too weak to be observed.

As discussed in § III, measurements of the singlet-triplet flux ratios provide important tests of the models, since these ratios are most sensitive to the strengths of the intercombination transitions. Unfortunately, it is at present still difficult to obtain accurate relative calibrations of, for example, the Swan and Phillips lines at high resolution. Low-resolution spectra covering a wider wavelength range may be more appropriate. Such spectra in the 5200–12,000 Å range have been obtained by Di Santi and Fink (1987) at various positions offset from the nucleus of comet Halley in 1985 and 1986. A detailed comparison of the present models with their data will be presented in a future paper (Fink *et al.* 1988).

V. CONCLUDING REMARKS

The models presented in this work are not inconsistent with high-resolution observations of C_2 in comet Halley, and suggest that resonance fluorescence is the dominant process that distributes the populations over the vibrational and rotational levels of C_2 in comets. The largest uncertainties in the models continue to be the $a\,^3\Pi_u$–$X\,^1\Sigma_g^+$ and $c\,^3\Sigma_u^+$–$X\,^1\Sigma_g^+$ intercombination transition moments, although considerable progress has been made by the calculations of Le Bourlot and Roueff (1986). It is unlikely that the detailed individual rotational line probabilities are large enough to mimic a constant value $|D_{a-X}|^2 \approx 10^{-6}$ a.u. From simple theoretical estimates, the $|D_{c-X}|^2$ transition moment is plausibly of the same order of magnitude as the value inferred from the observations for $A^{d-c}/A^{d-a} = 0.03$–0.1. Still, the theoretical estimates of both intercombination transition moments appear slightly too small to cool the rotational and vibrational population distributions to the observed temperatures. It would be desirable to extend the calculations of Le Bourlot and Roueff (1986) to rotational levels with J up to 60. A similar calculation is needed for the $c\,^3\Sigma_u^+$–$X\,^1\Sigma_g^+$ transition. Estimates of the spin-orbit matrix elements are already available from the detailed calculations by Klotz (1987). Together with the theoretical recipe outlined by Le Bourlot and Roueff (1986), these calculations appear straightforward, but computationally very intensive. They may eventually lead to a parameter-free model for the fluorescent excitation of cometary C_2. The adopted range of values for the strength of the $d\,^3\Pi_g$–$c\,^3\Sigma_u^+$ transition appears justified from the preliminary results of Klotz (1987). More accurate spectroscopic data for energy levels in the $c\,^3\Sigma_u^+$ state would be useful.

A novel feature of the models presented in this work is the inclusion of the rotational structure. The models predict that the rotational temperatures in the $d\,^3\Pi_g$ vibrational levels may differ significantly from the vibrational temperature, and that both temperatures may be different for the individual F_1, F_2, and F_3 electronic substates. The former prediction appears to be confirmed by the observations of comet Halley. In addition, important differences in the rotational excitation temperature have been found at the nucleus and at the coma position in comet Halley. It has been argued that these differences are most likely caused by shielding of the solar radiation by dust particles in the inner coma, although this explanation is not supported by the recent work of O'Dell *et al.* (1988). It is important to note that a number of cometary C_2 emission

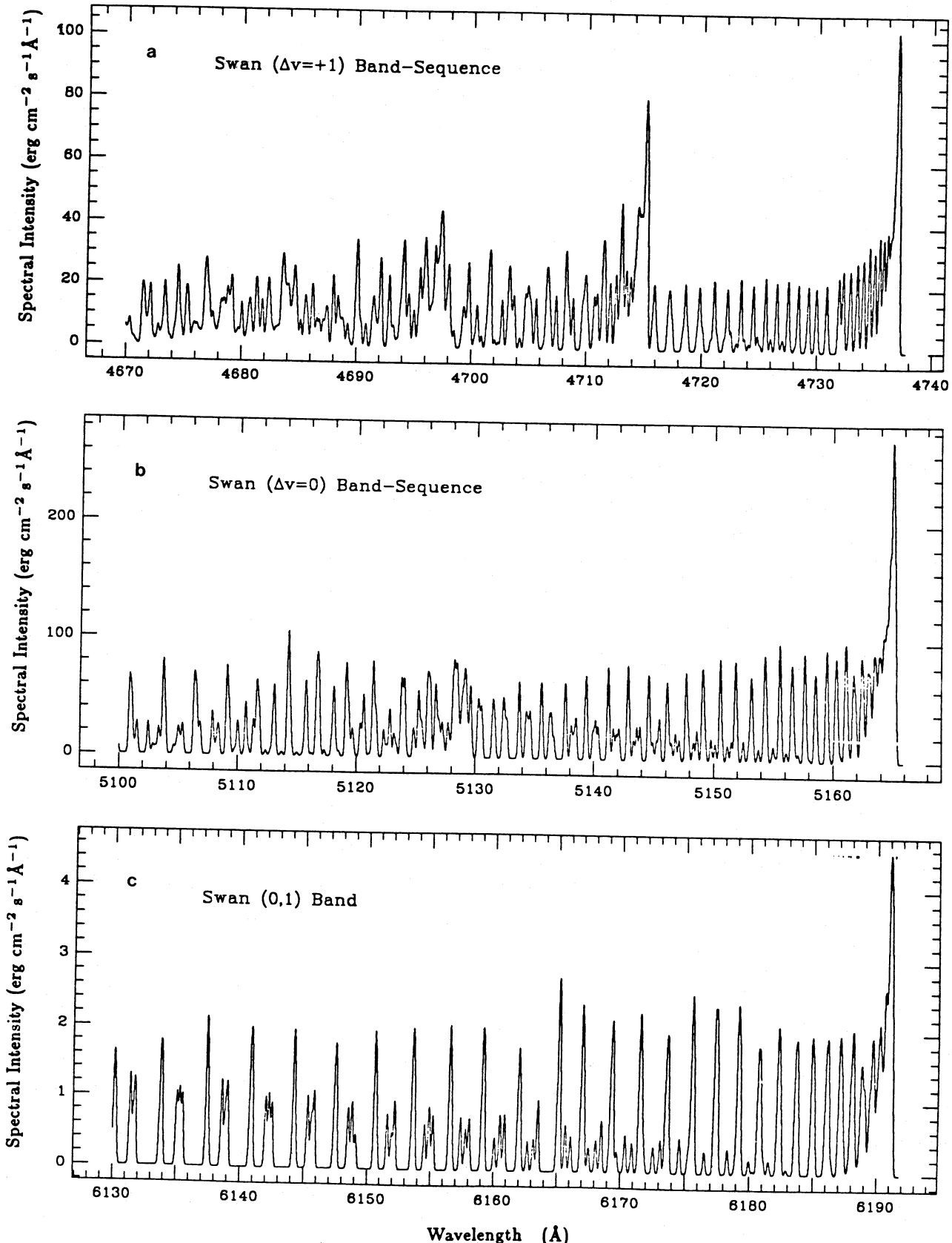

FIG. 5.—(*a*)–(*c*) Theoretical emission spectra of bands with $v' < 5$ in the $\Delta v = +1, 0$, and -1 Swan system at a resolution of 0.2 Å. For employed parameters, see Fig. 3. The absolute flux emitted by 10^{16} molecules into 4π sr is presented. (*d*)–(*f*) Theoretical emission spectra of the (2, 0) and (1, 0) Phillips system and the (2, 0) Ballik-Ramsay system at a resolution of 0.4 Å. For employed parameters, see Fig. 3.

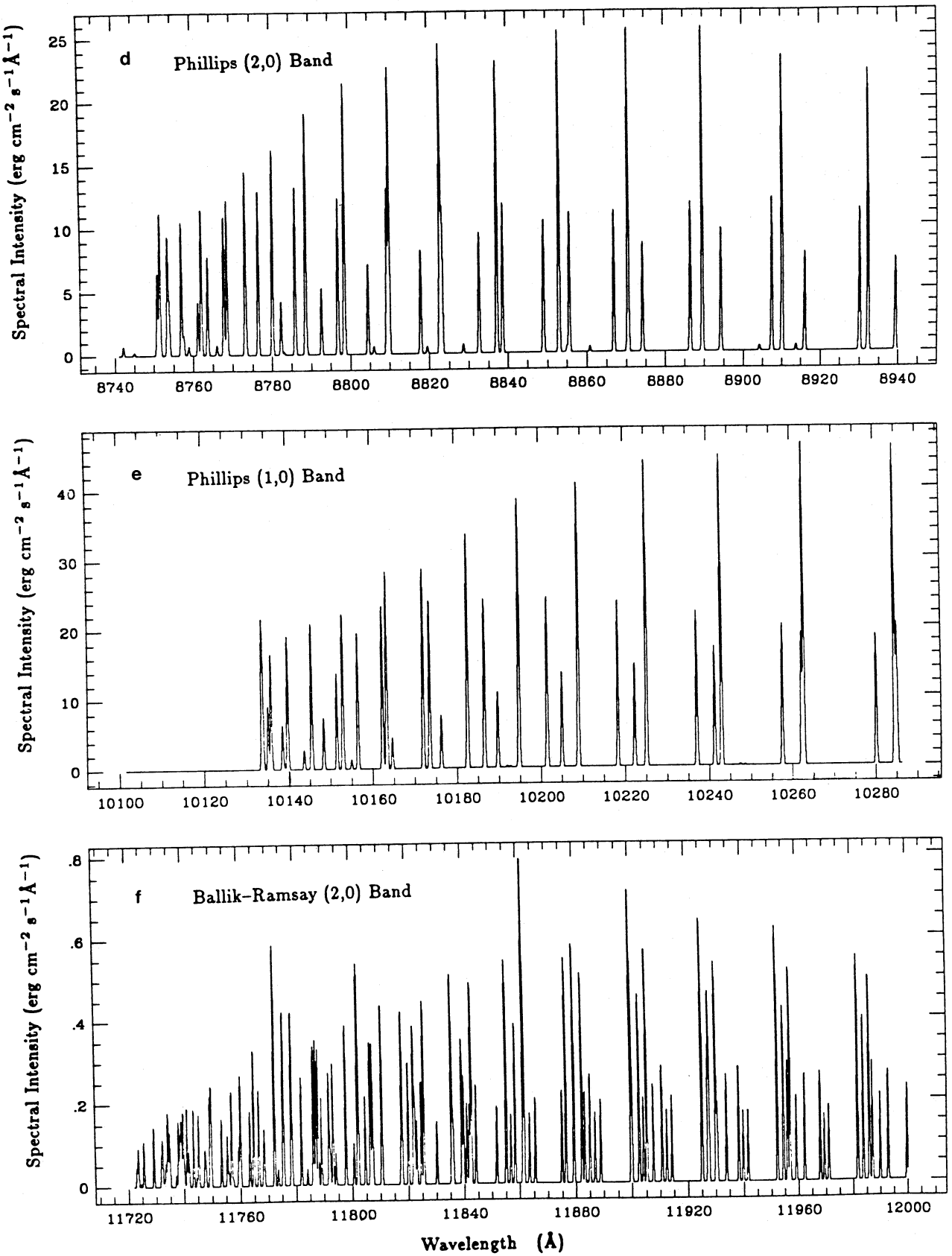

FIG. 5—*Continued*

spectra have been obtained at the nucleus position, but that previous analyses did not distinguish between the nucleus and coma positions. The only other comet so far for which high-resolution spectra are available is comet West (Lambert and Danks 1983). Their inferred $T_{\rm rot} \approx (3500 \pm 400)$ K at $\mathscr{R}_c = 0.78$ AU is not inconsistent with the present models, but their measured $T_{\rm vib} = T_{\rm rot}$ is significantly lower than the predicted value of $\sim$4800 K. However, comet West 1976 was one of the dustiest comets observed, and the measurements were performed close to the nucleus position. A decrease in vibrational and rotational temperatures of the order of 500 K or more is therefore not unlikely.

The models make clear predictions about the variations of the rotational and vibrational temperatures and the flux ratios in various transitions with heliocentric distance. However, for the most commonly observed flux ratios, such as those for bands in the Swan $\Delta v = 0$, 1, and -1 sequences, the variation is only of the order of 20%–50% over a wide range of parameter space. Such variations are usually comparable to the errors in the observed flux ratios, making it difficult to draw any firm conclusions. Accurate measurements of the Phillips/Swan flux ratios may indicate whether the employed intercombination transition moments are consistent, but their variation with heliocentric distance is also small. On the other hand, the decrease by almost 1000 K in vibrational and rotational temperatures between 0.5 and 1.5 AU should be observable. Continuous high-resolution observations of a single bright comet as it approaches or recedes from the Sun with a single instrument at positions offset from the nucleus should provide the most stringent tests of the current models.

We are grateful to R. Klotz for providing us with his calculations of the C_2 spin-orbit coupling matrix elements prior to publication, and to J. Le Bourlot and E. Roueff for sending their calculated $a\,^3\Pi_u$–$X\,^1\Sigma_g^+$ transition probabilities. We are indebted to R. L. Kurucz for a magnetic tape copy of the Solar Flux Atlas. We wish to thank P. Wehinger, S. Wyckoff, and B. A. Peterson, and U. Fink for lending their spectra on comet Halley for comparison with theory prior to publication. I. Appenzeller and G. Münch, S. C. Tegler and C. R. O'Dell, and S. V. ONeil and P. Rosmus are acknowledged for providing their preprints in advance of publication. We thank S. Wyckoff for sharing observing time, and the MMT staff for cheerful assistance in observing a low-redshift, nonstellar object all the way to the lower elevation limit of the telescope. This work was partly supported by the National Aeronautics and Space Administration (NASA) under grant No. NSG-7421 to the Smithsonian Astrophysical Observatory. One of us (R. G.) is also indebted to I. Shapiro for providing a Smithsonian Predoctoral Fellowship. The hospitality of the Institute for Advanced Study in Princeton and its partial support through NSF grant PHY-8620266 are gratefully acknowledged.

APPENDIX

METHOD OF SOLUTION

The following approximations were made in the solution of the more than 4000 linear equations that describe the population densities in the various C_2 vibration-rotation levels. Consider first only allowed electronic transitions involving the singlet rotational states. In statistical equilibrium, the population densities $n_X^{v''J''}$ and $n_A^{v'J'}$ of rotational levels $v'J'$ and $v''J''$ in the $X\,^1\Sigma_g^+$ and $A\,^1\Pi_u$ states are given by

$$n_X^{v''J''} \sum_{v'J'} (B^{\rm abs}_{v'J',v''j''}\rho_v + *) = \sum_{v'J'} n_A^{v'J'}(A_{v'J',v''J''} + B^{\rm em}_{v'J',v''J''}\rho_v)\,, \tag{A1}$$

$$n_A^{v'J'} \sum_{v''J''} (A_{v'J',v''J''} + B^{\rm em}_{v'J',v''J''}\rho_v + **) = \sum_{v''J''} n_X^{v''J''}(B^{\rm abs}_{v'J',v''J''}\rho_v + *)\,. \tag{A2}$$

The equations require no further explanation except that the two terms not explicitly shown and indicated by one asterisk (*) and two asterisks (**) correspond to $(A_{v'J',\tilde{v}''\tilde{J}''} + B^{\rm em}_{v'J',\tilde{v}''\tilde{J}''}\rho_v)$ and $B^{\rm abs}_{v'J',\tilde{v}''\tilde{J}''}\rho_v$, respectively, and describe transitions in the $X\,^1\Sigma_g^+$–$A\,^1\Pi_u$ system. They are zero unless the levels $\tilde{v}''\tilde{J}''$ in $X\,^1\Sigma_g^+$ lie energetically higher than $v'J'$ in $A\,^1\Pi_u$. In that case, the explicitly mentioned terms are zero, of course.

The rotational states in $A\,^1\Pi_u$ are not involved in any other transitions and can be eliminated from the equations. The resulting system of equations is conveniently written in terms of

$$\boldsymbol{S}\boldsymbol{n}_S = 0\,, \tag{A3}$$

where $\boldsymbol{n}_S$ equals the column vector of the singlet ground state levels $\boldsymbol{n}_S = (v''J'')$ and the matrix elements S^{ij} are given by

$$S^{ij} = \sum_{v'J'} (B^{\rm abs}_{v'J',i}\rho_v + *_i)\delta_{ij} - \sum_{v'J'} \frac{(B^{\rm abs}_{v'J',j}\rho_v + **_j)(A_{v'J',i} + B^{\rm em}_{v'J',i}\rho_v + *_i)}{\sum\limits_k (A_{v'J',k} + B^{\rm em}_{v'J',k}\rho_v + **_k)}\,, \tag{A4}$$

where the numbers i, j, and k indicate the rotational states in $X\,^1\Sigma_g^+$, and $*_i = (A_{v'J',i} + B^{\rm em}_{v'J',i}\rho_v)$, etc.

For the triplet states, it is convenient to include the $c\,^3\Sigma_u^+$ levels $\boldsymbol{n}_c$ into the triplet ground-state vector, since the $c\,^3\Sigma_u^+$ levels do not decay to lower triplet states, i.e., $\boldsymbol{n}_T = (\boldsymbol{n}_a, \boldsymbol{n}_c)$, where $\boldsymbol{n}_a$ contains the $a\,^3\Pi_u$ rotational levels. Following the procedure outlined for the singlet states, a similar result of the form

$$\boldsymbol{T}\boldsymbol{n}_T = 0 \tag{A5}$$

can be obtained. The number of triplet ground state levels is $\sim$1600, so that the matrix $\boldsymbol{T}$ is of order 1600 × 1600, which is still quite

large to handle conveniently. An approximation was therefore made which permitted the separation of the equations into three independent sets.

$$\boldsymbol{T}_i \boldsymbol{n}_{T,i} = 0 , \qquad i = 1, 3 , \tag{A6}$$

where $\boldsymbol{n}_{T,i}$ contains only the ground-state levels of a single electronic substate F_i of the $a\,^3\Pi_u$ and $c\,^3\Sigma_u^+$ states. The approximation consists of the neglect of all the satellite branches, i.e., transitions with $\Delta J \neq \Delta N$, and appears justified since satellite branches are very weak in $^3\Pi$–$^3\Pi$ transitions, whereas in $^3\Sigma$–$^3\Pi$ transitions they are comparable to the intensity of the main branches ($\Delta J = \Delta N$) only for very low J values. The contributions of the intercombination transitions were introduced in the following way:

$$\left(\boldsymbol{S} + \sum_{i=1}^{3} \boldsymbol{XX}_i\right)\boldsymbol{n}_S + \sum_{i=1}^{3} \boldsymbol{AX}_i \boldsymbol{n}_{T,i} = 0 , \tag{A7}$$

$$\boldsymbol{XA}_i \boldsymbol{n}_S + (\boldsymbol{T}_i + \boldsymbol{AA}_i)\boldsymbol{n}_{T,i} = 0 , \qquad i = 1, 3 . \tag{A8}$$

The individual matrix elements (l, m) for $\boldsymbol{XX}_i$, $\boldsymbol{XA}_i$, $\boldsymbol{AX}_i$, and $\boldsymbol{AA}_i$ are given by

$$\boldsymbol{XX}_i^{lm} = \sum_k A(l, k_i)\delta_{lm} , \tag{A9}$$

$$\boldsymbol{XA}_i^{lm} = -A(l, m_i) , \tag{A10}$$

$$\boldsymbol{AX}_i^{lm} = -A(m_i, l) , \tag{A11}$$

$$\boldsymbol{AA}_i^{lm} = \sum_k A(l_i, k)\delta_{lm} . \tag{A12}$$

The values $A(l, m)$ are the intercombination transition probabilities between two rotational levels l, m of the singlet and triplet ground-state vector, the upper level in the transition appearing first. For the triplet levels, the corresponding electronic substate is indicated by the subscript i. Elimination of the triplet ground states leads to the following equation that determines the population of the singlet ground state levels

$$\left\{\boldsymbol{S} + \sum_{i=1}^{3} [\boldsymbol{XXi} - \boldsymbol{AX}_i(\boldsymbol{T}_i + \boldsymbol{AA}_i)^{-1}\boldsymbol{XA}_i]\right\}\boldsymbol{n}_S = 0 . \tag{A13}$$

Equation (A13) can be solved for $\boldsymbol{n}_S$ by providing one more equation, for instance $\sum_i n_S^i = 1.0$. With the solution for the singlet ground states, the population distribution in the triplet ground states and finally in the excited singlet and triplet states can be successively reconstructed.

REFERENCES

A'Hearn, M. F. 1975, *A.J.*, **80**, 861.
———. 1978, *Ap. J.*, **219**, 768.
A'Hearn, M. F., and Feldman, P. D. 1980, *Ap. J. (Letters)*, **242**, L187.
A'Hearn, M. F., Thurber, C. H., and Millis, R. L. 1977, *A.J.*, **82**, 518.
Amiot, C. 1983, *Ap. J. Suppl.*, **52**, 329.
Appenzeller, I., and Münch, G. 1987, *Astr. Ap.*, **187**, 465.
Arpigny, C. 1965, *Ann. Rev. Astr. Ap.*, **3**, 351.
———. 1976, in *The Study of Comets*, ed. B. Bonn, M. Mumma, W. Jackson, M. A'Hearn, and R. Harrington (NASA SP-393), p. 797.
Arpigny, C., Dossin, F., Manfroid, J., Magain, P., Danks, A. C., Lambert, D. L., and Sterken, C. 1986, *The Messenger*, **45**, 9.
Bauer, W., Becker, K. H., Bielefeld, M., and Meuser, R. 1986, *Chem. Phys. Letters*, **123**, 33.
Bauer, W., Becker, K. H., Hubrich, C., Meuser, R., and Wildt, J. 1985, *Ap. J.*, **296**, 758.
Bleekrode, R., and Nieuwpoort, W. C. 1965, *J. Chem. Phys.*, **43**, 3680.
Chabalowski, C. F., Buenker, R. J., and Peyerimhoff, S. D. 1981, *Chem. Phys. Letters*, **83**, 441.
Chabalowski, C. F., Peyerimhoff, S. D., and Buenker, R. J. 1983, *Chem. Phys.*, **81**, 57.
Chauville, J., Maillard, J. P., and Mantz, A. W. 1977, *J. Molec. Spectrosc.*, **68**, 399.
Cochran, A. L. 1985, *Ap. J.*, **289**, 388.
Cooper, D. M., and Nicholls, R. W. 1975, *J. Quant. Spectrosc. Rad. Tranf.*, **15**, 139.
Danks, A. C., and Dennefeld, M. 1981, *A.J.*, **86**, 314.
Danks, A. C., Lambert, D. L., and Arpigny, C. 1974, *Ap. J.*, **194**, 745.
Danylewich, L. L., Nicholls, R. W., Neff, J. S., and Tatum, J. B. 1978, *Icarus*, **35**, 112.
Davis, S. P., Smith, W. H., Brault, J. W., Pecyner, R., and Wagner, J. 1984, *Ap. J.*, **287**, 455.
Di Santi, M., and Fink, U. 1987, private communication and in preparation.
Dressler, K., and Ramsay, D. A. 1959, *Phil. Trans. Roy. Soc. London, A*, **251**, 553.
Dwivedi, P. H., Branch, D., Huffaker, J. N., and Bell, R. A. 1978, *Ap. J. Suppl.*, **36**, 573.
Fink, U., *et al.* 1988, in preparation.
Gebel, W. L. 1970, *Ap. J.*, **161**, 765.
Gredel, R., van Dishoeck, E. F., and Black, J. H. 1989, in preparation.
Heubner, W. F. 1986, in *Molecular Astrophysics*, ed. G. H. F. Diercksen, W. F. Huebner, and P. W. Langhoff (Dordrecht: Reidel), p. 311.
James, T. C. 1971, *J. Chem. Phys.*, **55**, 4118.
Kirby, K., and Liu, B. 1979, *J. Chem. Phys.*, **70**, 893.
Klotz, R. 1987, private communication.
Kovács, J. 1969, *Rotational Structure in the Spectra of Diatomic Molecules* (London: Adam Hilger).
Krishna Swamy, K. S. 1986, *Pub. A.S.P.*, **98**, 252.
Krishna Swamy, K. S., and O'Dell, C. R. 1977, *Ap. J.*, **216**, 158.
———. 1979, *Ap. J.*, **231**, 624.
———. 1981, *Ap. J.*, **251**, 805.
———. 1987, *Ap. J.*, **317**, 543.
Kurucz, R. L., Furenlid, I., Brault, J., and Testerman, L. 1984, *Solar Flux Atlas from 296 nm to 1300 nm* (*Nat. Solar Obs. Atlas*, No. 1).
Labs, D., and Neckel, H. 1970, *Solar Phys.*, **15**, 79.
Lambert, D. L., and Danks, A. C. 1983, *Ap. J.*, **268**, 428.
Larsson, M. 1983, *Astr. Ap.*, **128**, 291.
Le Bourlot, J., and Roueff, E. 1986, *J. Molec. Spectrosc.*, **120**, 157.
Mayer, P., and O'Dell, C. R. 1968, *Ap. J.*, **153**, 951.
McFadden, L. A., A'Hearn, M. F., Feldman, P. D., Roettger, E. E., Edsall, D. M., and Butterworth, P. S. 1987, *Astr. Ap.*, **187**, 333.
Nieuwpoort, W. C., and Bleekrode, R. 1969, *J. Chem. Phys.*, **51**, 2051.
O'Dell, C. R. 1971, *Ap. J.*, **164**, 511.
O'Dell, C. R., Robinson, R. R., Krishna Swamy, K. S., McCarthy, P. J., and Spinrad, H. 1988, *Ap. J.*, **334**, 476.
ONeil, S. V., Rosmus, P., and Werner, H.-J. 1987, *J. Chem. Phys.*, **87**, 2847.
Owen, T. 1973, *Ap. J.*, **184**, 33.
Phillips, J. G. 1957, *Ap. J.*, **125**, 153.
———. 1968, *J. Molec. Spectrosc.*, **28**, 233.
Pouilly, B., Robbe, J. M., Schamps, J., and Roueff, E. 1983, *J. Phys. B.*, **16**, 437.
Roux, F., Wannous, G., Michaud, F., and Verges, J. 1985, *J. Molec. Spectrosc.*, **109**, 334.
Schadee, A. 1975, *Astr. Ap.*, **41**, 203.
———. 1978, *J. Quant. Spectrosc. Rad. Transf.*, **19**, 451.
Stark, G., and Davis, S. P. 1985, *Zs. Phys. A*, **321**, 75.
Stawikowski, A., and Greenstein, J. L. 1964, *Ap. J.*, **140**, 1280.
Stawikowski, A., and Swings, P. 1960, *Ann. d'Ap.*, **23**, 585.

Stockhausen, R. E., and Osterbrock, D. E. 1965, *Ap. J.*, **141**, 287.
Tatarczyk, T., Fink, E. H., and Becker, K. H. 1976, *Chem. Phys. Letters*, **40**, 126.
Tegler, S. C., and O'Dell, C. R. 1987, *Ap. J.*, **317**, 987.
van de Burgt, L. J., and Heaven, M. C. 1987, *J. Chem. Phys.*, **87**, 4235.
van Dishoeck, E. F. 1983, *Chem. Phys.*, **77**, 277.
Vanysek, V., Valniček, B., and Sudova, J. 1988, *Nature*, **333**, 435.
Wehinger, P. A., Peterson, B. A., Wyckoff, S., Lindholm, E., Gredel, R., van Dishoeck, E., and Black, J. H. 1986, in *Proc. 20th ESLAB Symposium on the Exploration of Halley's Comet*, (ESA SP-250), p. 475.
Wehinger, P. A., Peterson, B. A., Wyckoff, S., Lindholm, E., Gredel, R., van Dishoeck, E., and Black, J. H. 1989, in preparation.
Whiting, E. E. 1973, NASA TN D-7268.
Whiting, E. E., and Nicholls, R. W. 1974, *Ap. J. Suppl.*, **27**, 1.
Whiting, E. E., Paterson, J. A., Kovács, I., and Nicholls, R. W. 1973, *J. Molec. Spectrosc.*, **47**, 84.
Whiting, E. E., Schadee, A., Tatum, J. B., Hougen, J. T., and Nichols, R. W. 1980, *J. Molec. Spectrosc.*, **80**, 249.

JOHN H. BLACK: Steward Observatory, University of Arizona, Tucson, AZ 85721

ROLAND GREDEL: European Southern Observatory, Casilla 567, La Serena, Chile

EWINE F. VAN DISHOECK: Center for Cosmochemistry, Division of Geological and Planetary Sciences, California Institute of Technology 170-25, Pasadena, CA 91125